0-315-01187-4

I✹ National Library
of Canada

Bibliothèque nationale
du Canada

Canadian Theses Division   Division des thèses canadiennes

Ottawa, Canada
K1A 0N4   **49045**

PERMISSION TO MICROFILM — AUTORISATION DE MICROFILMER

- Please print or type — Écrire en lettres moulées ou dactylographier

Full Name of Author — Nom complet de l'auteur

Mary Margaret Morrison

Date of Birth — Date de naissance

Feb. 21, 1955

Country of Birth — Lieu de naissance

Canada

Permanent Address — Résidence fixe

991 Victoria Road
Sydney, Nova Scotia.
B1N 1K8.

Title of Thesis — Titre de la thèse

Infrared Spectra of Ammonia Hemihydrate
and Ammonia Monohydrate

University — Université

University of Alberta

Degree for which thesis was presented — Grade pour lequel cette thèse fut présentée

Master of Science

Year this degree conferred — Année d'obtention de ce grade

1980

Name of Supervisor — Nom du directeur de thèse

Dr. John E. Bertie

Date

Signature

NOTICE · AVIS

The quality of this microfiche is heavily dependent upon the quality of the original thesis submitted for microfilming. Every effort has been made to ensure the highest quality of reproduction possible.

If pages are missing, contact the university which granted the degree.

Some pages may have indistinct print especially if the original pages were typed with a poor typewriter ribbon or if the university sent us a poor photocopy.

Previously copyrighted materials (journal articles, published tests, etc.) are not filmed.

Reproduction in full or in part of this film is governed by the Canadian Copyright Act, R.S.C. 1970, c. C-30. Please read the authorization forms which accompany this thesis.

La qualité de cette microfiche dépend grandement de la qualité de la thèse soumise au microfilmage. Nous avons tout fait pour assurer une qualité supérieure de reproduction.

S'il manque des pages, veuillez communiquer avec l'université qui a conféré le grade.

La qualité d'impression de certaines pages peut laisser à désirer, surtout si les pages originales ont été dactylographiées à l'aide d'un ruban usé ou si l'université nous a fait parvenir une photocopie de mauvaise qualité.

Les documents qui font déjà l'objet d'un droit d'auteur (articles de revue, examens publiés, etc.) ne sont pas microfilmés.

La reproduction, même partielle, de ce microfilm est soumise à la Loi canadienne sur le droit d'auteur, SRC 1970, c. C-30. Veuillez prendre connaissance des formules d'autorisation qui accompagnent cette thèse.

THIS DISSERTATION HAS BEEN MICROFILMED EXACTLY AS RECEIVED

LA THÈSE A ÉTÉ MICROFILMÉE TELLE QUE NOUS L'AVONS REÇUE

THE UNIVERSITY OF ALBERTA

INFRARED SPECTRA OF AMMONIA HEMIHYDRATE

AND AMMONIA MONOHYDRATE

by

© MARY MARGARET MORRISON

A THESIS

SUBMITTED TO THE FACULTY OF GRADUATE

STUDIES AND RESEARCH IN PARTIAL

FULFILMENT OF THE REQUIREMENTS FOR THE

DEGREE OF MASTER OF SCIENCE

DEPARTMENT OF CHEMISTRY

EDMONTON, ALBERTA

FALL, 1980

THE UNIVERSITY OF ALBERTA

FACULTY OF GRADUATE STUDIES AND RESEARCH

The undersigned certify that they have read, and
recommend to the Faculty of Graduate Studies and Research,
for acceptance, a thesis entitled

'INFRARED SPECTRA OF AMMONIA HEMIHYDRATE

AND AMMONIA MONOHYDRATE'

submitted by MARY MARGARET MORRISON in partial
fulfilment of the requirements for the degree of
Master of Science.

....
Supervisor

....

....

DATE 6ᵃ October 1980.

TO MY FAMILY

ABSTRACT

Ammonia monohydrate and ammonia hemihydrate were prepared by mixing stoichiometric volumes of ammonia and water and freezing the solutions. They were characterized by means of X-ray powder-diffraction photographs. The mid-infrared spectra of ammonia monohydrate and ammonia hemihydrate at ~95°K were obtained and the assignments of the spectral features were made on the basis of site symmetry, with reference to the spectra of solid ammonia and ice. The spectra obtained are quite different from those reported by Waldron and Hornig in 1953 and it is believed that they did not obtain the spectra of the solid hydrates.

The spectra of the two hydrates show that the O-H stretching vibration in an O-H···N bond of length 2.775 to 2.85 Å at 95°K absorbs between 2910 and 3125 cm^{-1}. This information is valuable for making similar assignments in other compounds since general correlations of ν(O-H) with R(O-H···N) are not available. In particular, it confirms a recent assignment in the spectrum of hexamethylenetetramine hexahydrate.

Mid-infrared spectra of various isotopic forms of ammonia hemihydrate were also obtained. Frequencies of isolated N-H and N-D stretching vibrations of the ammonia molecules of type I and II are reported, as well as the symmetric deformation vibrations of isolated ND_2H and NH_2D.

Peaks due to isolated O-D stretching vibrations in the $O-D \cdots N_I$ and $O-D \cdots N_{II}$ hydrogen bonds as well as the O-H analogs, were identified. The frequencies of the features due to $\nu_R(HOD)$ were also obtained from a dilute deuterated sample.

Information obtained from the spectra of the isotopes led to the assignment of the $\nu_3(NH_3)$ and $\nu_3(ND_3)$ doublets to vibrations in the two different types of ammonia molecules in the crystal structure. The 10 cm^{-1} split of $\nu_2(NH_3)$ and $\nu_2(ND_3)$ is believed to be due to unit-cell-group splitting and the 30 cm^{-1} split of $\nu_2(NH_2D)$ and $\nu_2(ND_2H)$ is argued to be site splitting caused by the lowering of the symmetry of a C_{3v} molecule when placed in the crystal structure, coupled with very similar ν_2 vibration frequencies in the two types of ammonia molecule. Further work is suggested.

ACKNOWLEDGEMENTS

TABLE OF CONTENTS

LIST OF FIGURES

List of Figures, Continued

CHAPTER I.

INTRODUCTION

1.1 General Introduction

In a recent infrared study of hexamethylenetetramine nexahydrate (1), uncertainty arose in the assignment of the O-H stretching frequency of an O-H$\cdots$N bond of length 2.81 $\overset{o}{A}$. Very limited experimental evidence is available in the literature to support the assignment of this vibration at 3012 cm^{-1}. Nakamoto et al. (2) have published correlations of O-H$\cdots$N bond lengths with O-H stretching frequencies, but only for cyclic dimer systems of a particular type. These correlations clearly cannot be applied to the hexamethylenetetramine hexahydrate system (1). Thus, an infrared study of a simple molecular system having O-H$\cdots$N bonds would provide evidence for or against a frequency of 3012 cm^{-1} for such a bond of length 2.81 $\overset{o}{A}$.

The hydrates of ammonia, ammonia monohydrate ($NH_3 \cdot H_2O$) and ammonia hemihydrate ($2NH_3 \cdot H_2O$), seemed to be ideal compounds for this experiment. Their crystal structures have been reported (3,4) and it is known that they are simple molecular compounds containing bonds of the type O-H$\cdots$O, O-H$\cdots$N and N-H$\cdots$O. They are important in their own right as simple hydrogen-bonded crystals formed by two small molecules of chemical importance. Further,

it can realistically be hoped that quantum mechanical calculations of interacting ammonia and water molecules will soon be made with sufficient accuracy to enable them to be used to interpret the vibrational spectra of the solids. In time, high quality vibrational spectra of such solids will provide data with which to test such calculations. Only one attempt to obtain their vibrational spectra has been made (5), which is surprising for such simple solids but which is explained by the fact that they melt at -79°C (6) and are, thus, difficult to handle.

It should be noted that ammonia monohydrate is sometimes called ammonium hydroxide (NH_4OH) and ammonia hemihydrate is sometimes called ammonium oxide ($(NH_4)_2O$) in the literature (6,7,8). However, the former names are more appropriate since the compounds consist of hydrogen-bonded ammonia and water molecules (3,4) and will be used throughout this thesis.

This thesis presents the mid-infrared spectrum of ammonia monohydrate at 95°K and the mid-infrared spectra of ammonia hemihydrate in various isotopic forms at 95°K. The major subject of this thesis is the assignment of the spectrum of ammonia hemihydrate. This work led to obtaining the preliminary survey spectrum of ammonia monohydrate which is presented and discussed.

A review of the solid-liquid equilibrium diagram
for the ammonia-water system is presented in Section 1.2.
Thermodynamic properties, early mid-infrared work and
structural information concerning the solid hydrates are
reviewed in Section 1.3. Objectives of this study appear
in Section 1.4.

1.2 A Review of the Solid-Liquid Equilibrium Diagram
of the Ammonia-Water System

The solid hydrates of ammonia having the theoretical
compositions, 48.59 weight % NH_3 corresponding to
ammonia monohydrate and 65.4 weight % NH_3 cor-
responding to ammonia hemihydrate, were first isolated
by Frank Rupert (7) in 1909. Rupert presented a solid-
liquid equilibrium diagram based on freezing point deter-
minations as a function of composition of ammonia-water
solutions. This diagram showed two maxima corresponding
to the formation of the two hydrates of ammonia. Since
1909, this work has been repeated by several authors
(8-16), each confirming the existence of the hydrates.
The melting points and eutectic points determined by
these authors are summarized in Table 1.1 along with
Rupert's values. A representative diagram, temperature
versus composition, of the ammonia-water system is shown
in Figure 1.1. Postma's (12) fusion curve has been
selected as his melting points and eutectic points have
been more recently confirmed by Hildenbrand and Giauque

TABLE 1.1

Melting Points and Eutectic Points of the Ammonia-Water System

	Rupert [8]		Baume and Tykociner [11]		Postma [12]		Elliott [13]		Hildenbrand and Giauque [6]		Mironov [14]		Rollet and Vuillard [15,16]	
	Weight% NH_3	Temp. (°C)	Weight% NH_3	Temp. (°C)	Weight% NH_3	Temp. (°C)	Weight% NH_3	Temp. (°C)	Weight% NH_3	Temp. (°C)	Weight% NH_3	Temp. (°C)	Weight% NH_3	Temp. (°C)
$H_2O-NH_3\cdot2H_2O$													32.9	-98.0
$NH_3\cdot2H_2O-NH_3\cdot H_2O$													35.3	-98.8
$H_2O-NH_3\cdot H_2O$	-34	<-120	34.3	-100.9	33.4	-100.3	31.3	-102.5			32.7	-101.3	33.9	-103.3
$NH_3\cdot H_2O$	48.6	-79	48.6	-79.5	48.6	-79.0	48.6	-79.0	48.6	-79.01	48.6	-77.0	48.6	-79.0
$NH_3\cdot H_2O-2NH_3\cdot H_2O$	56.5	-87	56.7	-87.3	57.1	-86.0	57.7	-88.2		-85.8	56.7	-85.4		
$2NH_3\cdot H_2O$	65.4	-79	65.4	-79.4	65.4	-78.8	65.4	-78.6	65.4	-78.84	65.4	-77.4		
$2NH_3\cdot H_2O-NH_3$	80.3	-94	79.8	-92.6	80.5	-92.5	78.4	-94.7		-92.0	79.9	-92.2		

*Data calculated from respective graphs by Mironov (14).
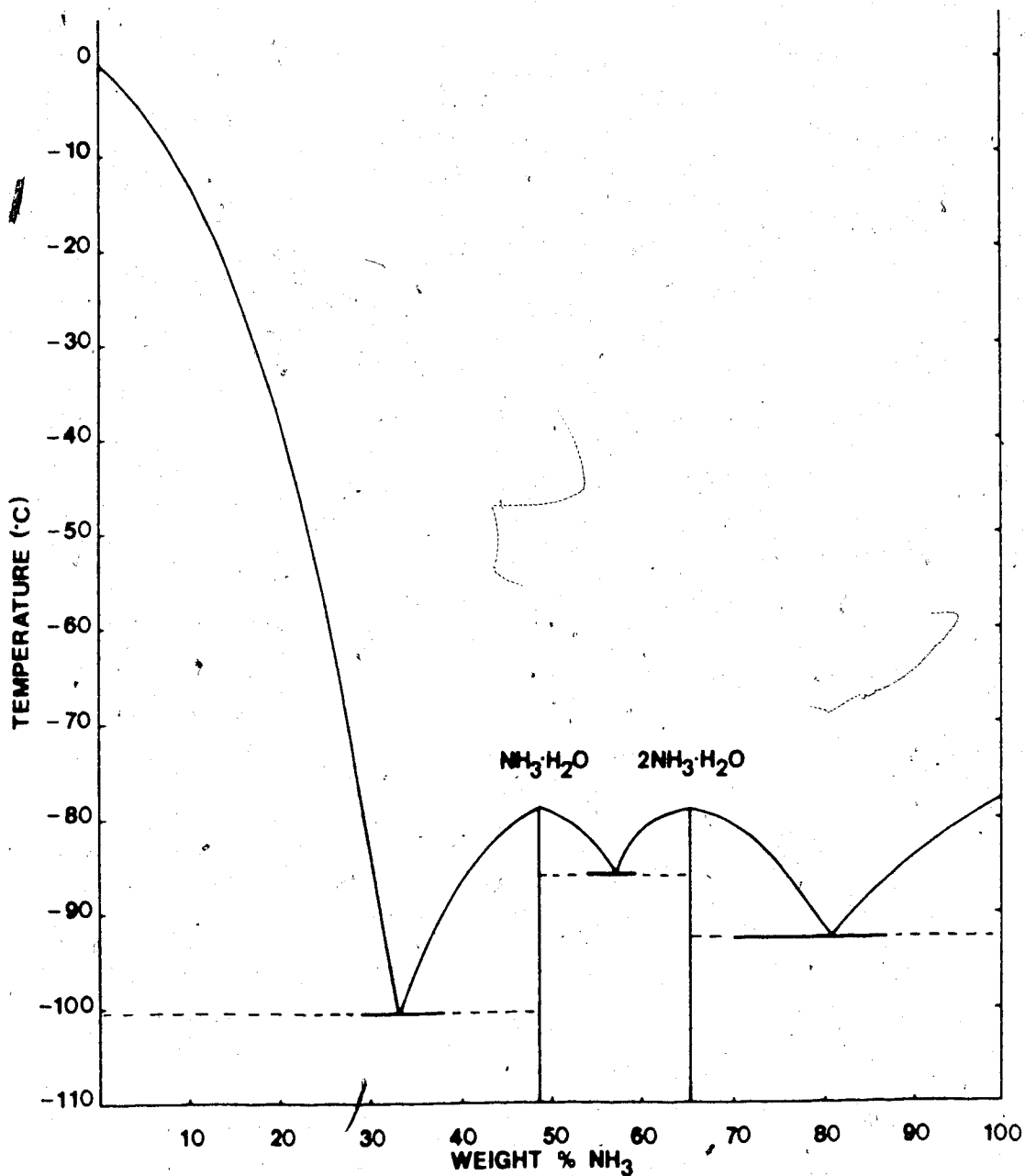
Figure 1.1 General solid-liquid equilibrium diagram for the ammonia-water system. From Postma (12) with compositions converted to weight % NH_3 from mole % NH_3. The melting points of $NH_3 \cdot H_2O$ and $2NH_3 \cdot H_2O$ are -79.0 and -78.8°C, respectively. The eutectic points are at 33.4% NH_3, -100.3°C; 57.1% NH_3, -86.0°C; 80.5% NH_3, -92.5°C. The dashed lines are extrapolations.

(6) whose determinations are also listed in Table 1.1.

In most cases, the eutectic, ice-$NH_3 \cdot H_2O$, has not been determined experimentally since high viscosity and supercooling hinders crystallization in the composition range ~28-34 weight % NH_3. Most of the eutectic temperatures and compositions listed in Table 1.1 for this region have been determined either graphically, by extrapolation of the liquidus curve to a point of intersection or by measuring the temperature at which the last crystals disappear under slow heating.

In 1923, Fritz Friedrichs (17) suggested a continuous series of mixed crystals or solid solutions existed instead of two discrete hydrates. In 1924, Elliott (13) claimed the existence of discrete compounds was proved by his visual inspection of the crystals upon formation. In 1954, Mironov (14) undertook a systematic study of the problem. To that date, only a few points of the solidus curve had been determined (12). Mironov attempted to disprove the existence of solid solutions by determining enough points of the solidus curve to show that this curve changed temperature only at the congruent melting points.

Mironov used thermal analysis, that is, cooling and heating curves, to determine temperatures on the liquidus and solidus curves for particular compositions. He obtained data to fill in the missing solidus points for

all regions except for 0-32.7 weight % NH_3 where crystallization difficulties prevented further experimentation. Mironov concluded, however, that Friedrichs was wrong and that a continuous series of mixed crystals did not exist. It should be noted that the temperatures Mironov obtained, listed in Table 1.1, are about 2° higher than the temperatures reported by other authors. Mironov made a significant contribution by providing data for the 32.7-48 weight % NH_3 region; thus, enabling the construction of the solidus curve at -101.3°C (or -103.3°C, if corrected for the systematic 2° error) for this region.

In this study, Mironov also determined a metastable point at 50.1 weight % NH_3 and -99°C. He predicted that extrapolation of the liquidus curve of $2NH_3 \cdot H_2O$ through this point would intersect with the extrapolated liquidus of H_2O to form a metastable eutectic at ~-127°C between 30 and 40 weight % NH_3.

In 1956, Rollet and Vuillard (15,16), as a result of their study of the vitreous state and the crystallization of aqueous solutions, discovered a new hydrate, $NH_3 \cdot 2H_2O$. Earlier workers had indicated that crystallization was difficult for ammonia-water mixtures having concentrations between 28 and 34 weight % NH_3. Rollet and Vuillard observed that crystallization could be induced by slowly heating a solution which had been vitri-

fied. With this method as well as the use of differential thermal analysis, they were able to establish a more detailed equilibrium diagram (Figure 1.2) of the ammonia-water system.

Rollet and Vuillard followed the thermal behavior of vitrified solutions by means of heating curves. They observed a glass transition from the vitreous state to the liquid state near -145°C for concentrations up to 42 weight % NH_3. Vitreous transformation for higher ammonia concentrations could not be determined with certainty. Upon further heating, crystallization of the mixture began at -115°C and led to a eutectic plateau at -103.3°C where the crystals melted. Rollet and Vuillard proved that this eutectic is metastable and at the same temperature for compositions from 1 to 48 weight % NH_3. They postulated that it is the ice-$NH_3 \cdot H_2O$ eutectic. The heating curve shows that this metastable eutectic is interrupted by the crystallization of a new species, which is immediately followed by a stable eutectic plateau at -98.0°C for dilute solutions and -98.8°C for concentrations of 33 to 48 weight % NH_3. To determine the eutectic composition of the new species, the length of the plateau, at -98.0°C or -98.8°C, in the heating curve was plotted against composition. The maxima obtained indicated that the eutectic composition was between 31.5 and 32.2 weight % NH_3. It was concluded that the new hydrate was
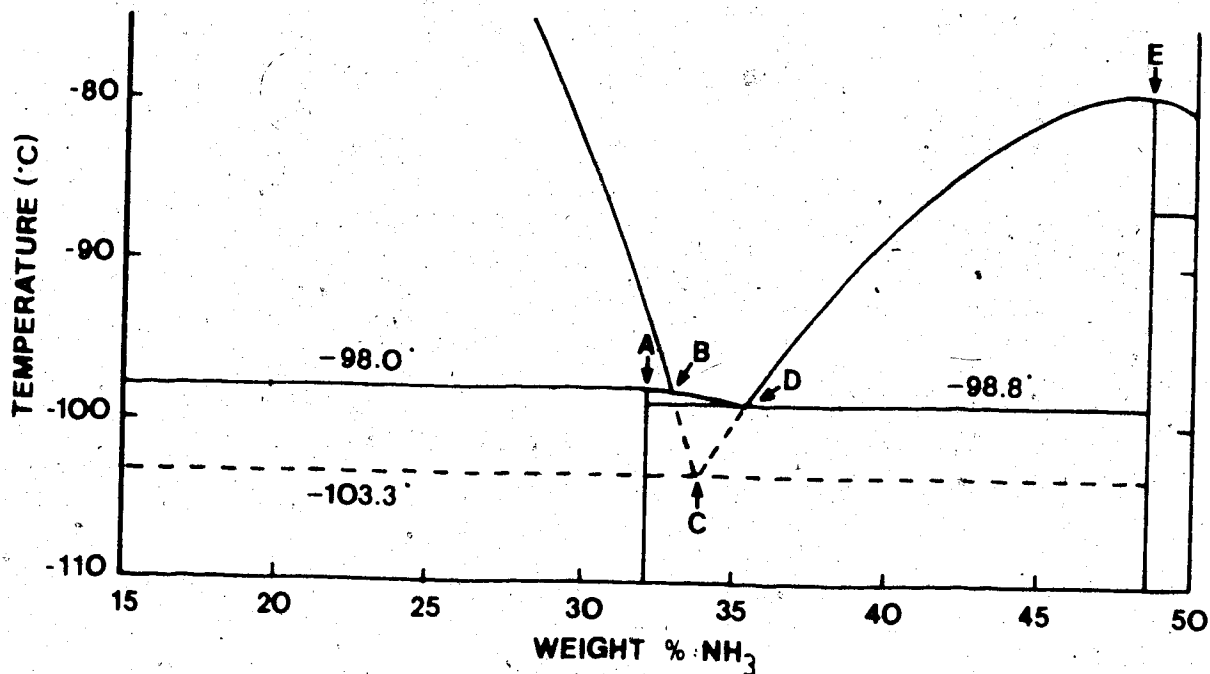
Figure 1.2 Detailed solid-liquid equilibrium diagram for
dilute solutions of NH_3 and H_2O. From Rollet and Vuillard
(15,16).
A) $NH_3 \cdot 2H_2O$ (32.2% NH_3) Melting point at -98.0 or -98.8°C.
B) ice -$NH_3 \cdot 2H_2O$ (32.9% NH3) Peritectic transition at -98.0°C.
C) ice - $NH_3 \cdot H_2O$ (33.9% NH_3) Metastable eutectic at -103.3°C.
D) $NH_3 \cdot 2H_2O$ - $NH_3 \cdot H_2O$ (35.3% NH_3) Stable eutectic at -98.8°C.
E) $NH_3 \cdot H_2O$ (48.57% NH_3) Melting point at -79.0°C.

$NH_3 \cdot 2H_2O$ which has a theoretical composition of 32.1 weight % NH_3.

A transition point, indicated in Figure 1.2, occurs at -98.0°C and 32.9 weight % NH_3. This transition point corresponds to the peritectic transformation, that is, incongruent melting of solid $NH_3 \cdot 2H_2O$ to yield ice plus liquid. The results of Rollet and Vuillard are also summarized in Table 1.1.

Van Kasteren (18) has recently published a similar, but far less extensive study than that of Rollet and Vuillard (15,16) apparently unaware of their study.

1.3 A Review of the Structural and Physical Properties of the Ammonia Hydrates

In 1953, Hildenbrand and Giauque (6) studied some thermodynamic properties of ammonia hemihydrate and ammonia monohydrate from 15 to 300°K. They were investigating possible disorder caused by random hydrogen bonding in the solid state at low temperatures.

One of their studies involved the measurement of the heats of fusion of the $NH_3-2NH_3 \cdot H_2O$ eutectic and the $2NH_3 \cdot H_2O-NH_3 \cdot H_2O$ eutectic. Their results indicated that the $2NH_3 \cdot H_2O$ phase has the same composition at each eutectic point within 0.02 mole percent. Although $NH_3 \cdot H_2O$ was not studied in such detail, measurements of the heat of fusion for this solid indicated that it is a pure compound to within about 0.05 mole percent.

The heats of fusion measured at the melting points of the two hydrates were: 9840 J mole^{-1} for $2NH_3 \cdot H_2O$ at $-78.84°C$ and 6560 J mole^{-1} for $NH_3 \cdot H_2O$ at $-79.01°C$.

Heat capacities of $2NH_3 \cdot H_2O$ were measured from 15 to 273°K and those of $NH_3 \cdot H_2O$ from 15 to 293°K. The heat capacity of $2NH_3 \cdot H_2O$ behaved anomalously in that two maxima appeared near 52°K. Hildenbrand and Giauque tried to explain the multiple maxima as being due to angular motions of the ammonia groups in more than one crystal plane or possibly due to two structurally different ammonia groups.

The entropies of ammonia hemihydrate and ammonia monohydrate were calculated to be 63.94 and 39.57 cal deg^{-1} mole^{-1}, respectively, at 298.16°K. It was concluded that the entropies of both compounds approach zero at 0°K within 0.1 cal deg^{-1} mole^{-1}. Hence, the crystalline states of $2NH_3 \cdot H_2O$ and $NH_3 \cdot H_2O$ at low temperatures were considered to be essentially ordered, including the hydrogen bonding.

The only infrared spectra of the crystalline ammonia hydrates reported in the literature are the work of Waldron and Hornig (5), published in 1953 for the range 3600-800 cm^{-1}. The method of sample preparation used by these authors was the condensation of ammonia and water vapor onto liquid-nitrogen-cooled NaCl and KBr plates. The spectra obtained were reported to resemble the spec-

trum of ice and the spectrum of crystalline ammonia. It seems unlikely that Waldron and Hornig could have obtained the correct phases at -195°C.

With no knowledge of the structure of the solid hydrates available, Waldron and Hornig drew several conclusions concerning the structure from the comparison of their spectra with those of solid ammonia, ice and an ammonium salt. They concluded that the hydrates were molecular rather than ionic because of the absence of the 1400 cm^{-1} bending vibration of NH_4^+. They also suggested the existence of an O-H$\cdots$N bond, since they believed that the water molecules were not so tightly bound as in ice because of the absence of the 812 cm^{-1} ice band. Waldron and Hornig reported the symmetrical bending vibration of ammonia to be at 1102 cm^{-1} in $NH_3 \cdot H_2O$ and to be a doublet, at 1020 and 1091 cm^{-1} in $2NH_3 \cdot H_2O$. They believed that the doublet indicated the possible existence of two structurally different ammonia molecules as suggested by Hildenbrand and Giauque (6). The 2950 cm^{-1} peak which appeared in the spectrum of both hydrates was attributed to an N-H$\cdots$O type bond and the 3140 cm^{-1} peak which appeared for the $2NH_3 \cdot H_2O$ was believed to be due to a weaker bond of the same type. Peaks at 3220 and 3365 cm^{-1} were believed to be due to mixed contributions of hydrogen bonded O-H and N-H vibrations.

Subsequent to the work of Waldron and Hornig, the crystal structure of ammonia hemihydrate was studied in 1953 by Siemons and Templeton (4) by means of single crystal X-ray diffraction. Ammonia hemihydrate was found to crystallize in the orthorhombic system with space group Pnma (19) and lattice constants $a = c = 8.41 \pm 0.03 \, \AA$ and $b = 5.33 \pm 0.02 \, \AA$ at $-95 \pm 10°C$. Assuming four molecules of $2NH_3 \cdot H_2O$ per unit cell, the density of the solid was calculated to be $0.916 \, g \, cm^{-3}$. This was acceptable compared to the rough value of $>0.8 \, g \, cm^{-3}$ measured for liquid $2NH_3 \cdot H_2O$ near the melting point.

The structure of ammonia hemihydrate was found to consist of alternating nitrogen and oxygen atoms connected by hydrogen bonds of the $O-H \cdots N$ and $N-H \cdots O$ type. These atoms form a cage-like cavity similar to a clathrate structure (20) and in the cavities sit a second type of ammonia molecule connected to one water molecule by an $O-H \cdots N$ hydrogen bond. Siemons and Templeton called the nitrogen atom of this latter type of ammonia, N_{II} and the other nitrogen, N_I. The hydrogens on N_{II} are unbonded and this ammonia molecule is believed to rotate freely about its $O-H \cdots N$ hydrogen bond. The suggestion of free rotation was supported by electron density maps which indicated more violent thermal motion at N_{II} than at N_I; and by the transitions observed by Hildenbrand and Giauque (6) at $52°K$. Hildenbrand and Giauque also indicated a

possible change in volume accompanying this transition. Siemons and Templeton noted that the angle between the O-H···N bonds at the water molecule, 116°, which is larger than expected for water, may be smaller below the ·52°K transition.

The geometry of the structure essentially dictates an ordered arrangement under Pnma symmetry of the hydrogen atoms that are not on $N_{II}H_3$. Siemons and Templeton also assumed that the average positions of the N_{II} hydrogen atoms had Pnma symmetry. Hydrogen bonds of lengths 2.83 Å for N_I···HO and 2.85 Å for N_{II}···HO are formed. The two free electron pairs of each oxygen atom accept three hydrogen bonds from ammonia, of lengths 3.11, 3.24 and 3.24 Å, each sharing two-thirds of an electron pair. Thus, each water molecule in the structure is five coordinated.

The crystal structure of ammonia monohydrate was studied by Olovsson and Templeton (3) in 1959. Single crystal X-ray studies at -95 and -160°C yielded the same structure, orthorhombic and in the space group $P2_12_12_1$. The unit cell parameters at -160°C were a = 4.51±0.01, b = 5.587±0.003 and c = 9.700±0.005 Å. Assuming four molecules of $NH_3 \cdot H_2O$ per unit cell, the density of the solid was calculated to be 0.95 g cm^{-3} at -160°C which is reasonable compared to 0.89 g cm^{-3}, measured by Hildenbrand and Giauque, for the liquid at -68°C.

The monohydrate was found to consist of planar zig-
zag chains of water molecules connected by hydrogen bonds.
The chain axes lie along the a axis of the unit cell in
approximately the z = 0 and z = ½ planes. The chains are
crosslinked by ammonia molecules via short, O-H···N,
hydrogen bonds of length 2.78 Å and via long, NH···O,
hydrogen bonds of lengths 3.21, 3.26 and 3.29 Å. To each
long bond, oxygen contributes one-third of an electron
pair. The oxygen atom of the water molecule is six coor-
dinated. It forms the four bonds mentioned above, as
well as two short bonds, to the two adjacent oxygen atoms
in the chain, of the type O-H···O and O···HO, both of
length 2.76 Å. The hydrogen atoms involved in these bonds
between oxygen atoms in the chain have not been located.
A large deviation of the angles between the long bonds
from the tetrahedral value indicate that the hydrogen
atoms may not lie on the lines joining nitrogen and oxy-
gen atoms. Rotation about the three-fold axis of ammonia
is believed to be prevented in the monohydrate by the
hydrogen bonding.

Additional evidence concerning the structure of
ammonia hemihydrate resulted from a ^{14}N nuclear quadrupole
resonance study by S. Eletr and C.T. O'Konski (21) in
1971. Four absorption frequencies were observed at 77°K.
These frequencies were paired by their Zeeman behavior,
confirming that two non-equivalent lattice sites are

occupied by ammonia. The temperature dependence of these frequencies was measured from 77 to 190°K. One pair of temperature dependence curves was much steeper than the other pair and was, therefore, assigned to the nitrogen designated N_{II}, since this nitrogen is believed to undergo greater thermal motion. The NQR studies also support the conclusion by Waldron and Hornig of the absence of ammonium ion in the compound. Such an ion would have a nearly zero quadrupole coupling constant because of the tetrahedral symmetry.

1.4 Objectives

Very little is known about the vibrational spectra of the crystalline hydrates of ammonia. The only spectra reported to date are the infrared spectra in the range 3600-800 cm^{-1} obtained by Waldron and Hornig (5). The validity of these spectra are in question because of the trial and error method of sample preparation, that is, the low temperature at which the molecules were mixed in the condensation of ammonia and water vapor in various proportions onto a cold plate.

Thus, the objective of this work is to obtain mid-infrared spectra of authentic samples of ammonia hemihydrate, $2NH_3 \cdot H_2O$, and several of its isotopic forms and to make a detailed assignment of the vibrational spectra. The method of preparation, to be described in Chapter II, is such that the sample can be characterized by X-ray

powder diffraction so that there will be no doubt as to

the identity of the sample used to obtain spectra.

A secondary objective in this work is to obtain the

mid-infrared spectrum of ammonia monohydrate, $NH_3 \cdot H_2O$.

The monohydrate is a possible impurity in the hemihydrate

preparation. Its spectrum is, therefore, necessary to

identify impurity peaks in the ammonia hemihydrate spec-

tra as well as being of interest in its own right.

CHAPTER II.

EXPERIMENTAL TECHNIQUES

2.1 Introduction

This chapter describes the experimental methods used to obtain the mid-infrared spectra of ammonia monohydrate and of ammonia hemihydrate in various isotopic forms. A low temperature mulling technique, developed by Bertie and Whalley (22), was used to prepare the samples for investigation at $95 \pm 10°K$.

Since ammonia monohydrate was a possible impurity, it was also prepared and its infrared spectrum was obtained. Ammonia monohydrate was not studied extensively for this thesis but was useful for the identification of impurity absorption in the hemihydrate spectra.

2.2 Chemicals

Anhydrous ammonia (99.99 mole %) was obtained from Matheson of Canada, Ltd. The purity of the ammonia gas was checked by taking its infrared spectrum. The only impurity detected was a small amount of carbon dioxide which was separated from the ammonia by distillation from a 1-chlorobutane slush at $-123°C$. Ammonia-d_3 (99 atom % D) and ammonia-^{15}N (99 atom % ^{15}N) were obtained from Merck, Sharp and Dohme, Can. Ltd. and were used as supplied.

Triply distilled water was obtained from the laboratory of Dr. H.B. Dunford. The deuterium oxide was obtained from a bottle in the laboratory. It was checked for isotopic purity by comparing its n.m.r. spectrum with that of solutions made by dissolving 1 mole % and 2 mole % of H_2O in it, with 99.96% D_2O taken from a freshly opened bottle obtained from the n.m.r. laboratory and with 99.7% D_2O obtained from Spectral Services. The relative integrated intensities of the residual H in the different solutions agreed with the nominal concentrations if the isotopic purity of the D_2O used was $99.5 \pm 0.1\%$.

The mulling agents were commercial propane (99.99 mole %), propylene (99.99 mole %) and chlorotrifluoromethane (99.0 mole %), used as supplied in one or four pound cylinders.

2.3 Sample Handling

Since the ammonia hydrates melt at -79°C, all manipulation of the samples was done in a cold can. The cold can is an uninsulated metal can in which liquid nitrogen boils rapidly to produce a cold, dry atmosphere. The lower half of the can is cylindrical but a side arm extends from the upper half. The can contains a brass table which serves as a working area for sample handling. The can is filled by pouring liquid nitrogen into the top of the can, or by filling a side reservoir which is connected to the can, until the level of liquid nitrogen

is just below the top of the table. Long-handled tools required for sample handling were usually set on the cold can table to cool to liquid-nitrogen temperature before use. A sample could be handled, with spatulae and tweezers, while it was at approximately 100°K without being contaminated by condensation. Plexiglass covers, placed on top of the cold can, helped to prevent condensation inside the can. Rubber gloves were always worn when working with the cold can to provide protection from the cold metal tools and to prevent condensation, in the can, of moisture from the hands.

2.4 Preparation of Ammonia Hemihydrate and its Isotopic Forms

For sample preparation, the necessary apparatus was connected to the vacuum line as illustrated in Fig. 2.1. Stoichiometric volumes of water and ammonia (Table 2.1) were calculated using the density of water at 20°C, 0.99823 g cm^{-3} (23), and the density of liquid ammonia at -70°C, 0.7253 g cm^{-3} (24).

To prepare the ammonia hemihydrate, the calculated volume of triply distilled water was syringed into the ball joint test tube, A in Figure 2.1. This test tube was attached to the vacuum line and the water was degassed by four freeze-pump-thaw cycles. The water was then distilled into the evacuated system, B, (Fig. 2.1), a test tube with a ground glass joint connected to the vacuum
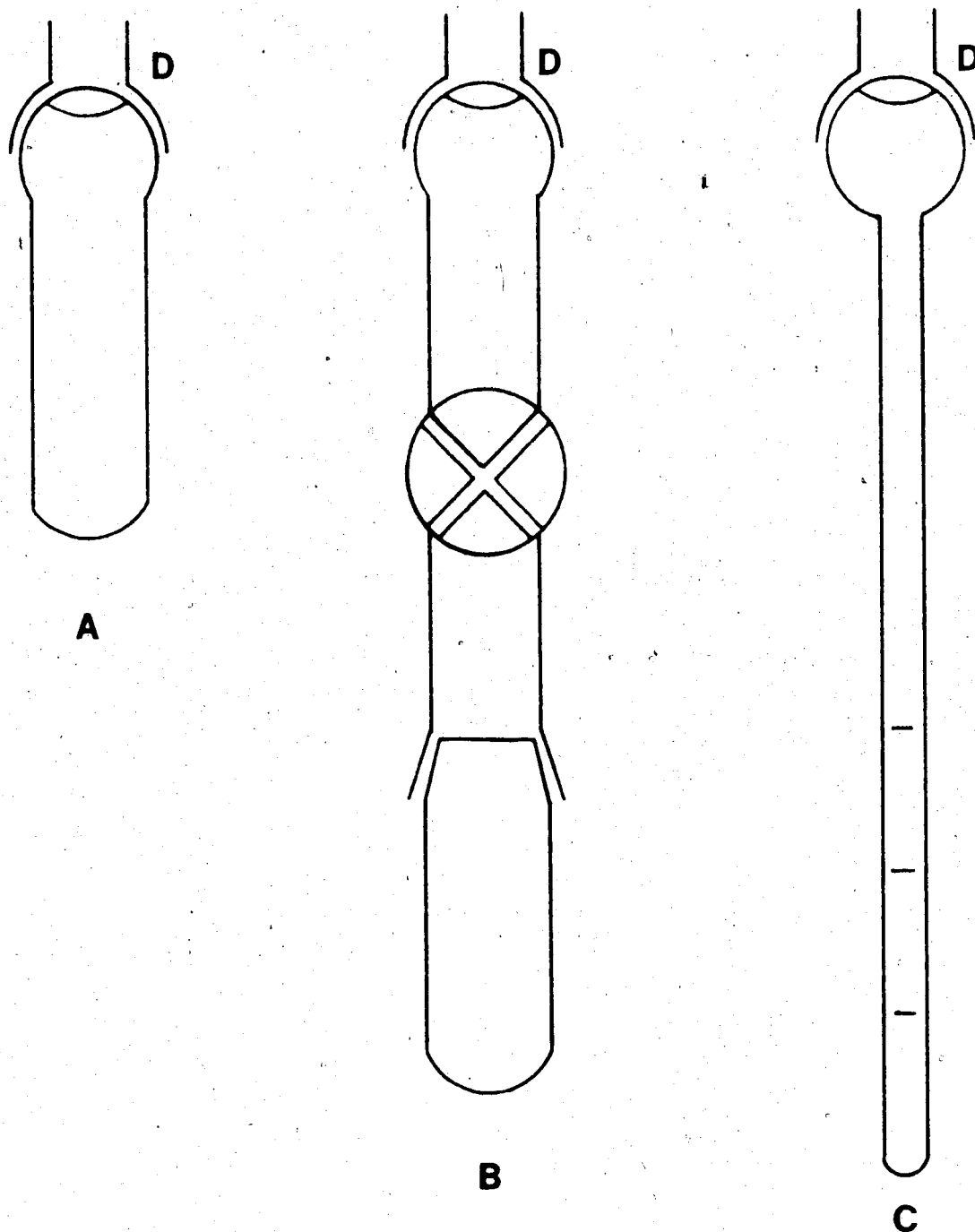
Figure 2.1 Apparatus used for preparation of the ammonia
hydrates. A) H_2O test tube, B) ground-glass-joint test
tube attached to a vacuum line connector equipped with a
stopcock, C) test tube for volume measurement of NH_3,
D) connection to the manifold of the vacuum line.

TABLE 2.1

Volumes Used for Sample Preparations

Sample Code	Sample	Volume of NH_3(ml)	Volume of H_2O (ml)	Volume of D_2O(ml)	Impurities[c]
S019-22	$2NH_3 \cdot H_2O$	3.0	1.16	-	$NH_3 \cdot H_2O$
S039	$2NH_3 \cdot H_2O$	0.50	0.180	-	$NH_3 \cdot H_2O$
S023-24	$2NH_3 \cdot H_2O$(5%D)	3.0	0.91	0.23	NH_3
S029-31	$2NH_3 \cdot H_2O$(10%D)	3.0	0.69	0.46	None Observed
S034-35	$2ND_3 \cdot D_2O$	1.00[a]	-	0.38	None Observed
S036	$2ND_3 \cdot D_2O$(5%H)	1.00[a]	0.080	0.30	None Observed
S037-38	$2^{15}NH_3 \cdot H_2O$	0.50[b]	0.192	-	$^{15}NH_3 \cdot H_2O$
S040	$2^{15}NH_3 \cdot H_2O$	0.25[b]	0.090	-	$^{15}NH_3 \cdot H_2O$
S025-28	$NH_3 \cdot H_2O$	3.0	2.31	-	ice, $2NH_3 \cdot H_2O$
S032-33	$NH_3 \cdot H_2O$	1.00	0.77	-	ice, $2NH_3 \cdot H_2O$

[a] ND_3 is substituted for NH_3.

[b] $^{15}NH_3$ is substituted for NH_3.

[c] Trace impurities were identified in the X-ray diffraction photographs but no spectral evidence of impurities was observed except for S039 and the $2^{15}NH_3 \cdot H_2O$ samples where $NH_3 \cdot H_2O$ or $^{15}NH_3 \cdot H_2O$ features were identified in the spectra.

line via a stopcock. The required volume of ammonia was condensed into a calibrated capillary tube, C in Fig. 2.1. The tube had been calibrated by syringing specific volumes of water into it. A cold methanol bath was used to control the temperature. At -70°C, the volume of ammonia was adjusted to the calibrated mark and the stopcock was closed. After evacuating the manifold, the ammonia was distilled into B, which contained the water. The stopcock of apparatus B was then closed and the apparatus was removed from the vacuum line.

At this point, the sample consisted of a layer of ice and a layer of solid ammonia. A chlorobenzene slush bath was used to warm the sample to approximately -45°C to melt the solid ammonia. Once melted, the ammonia was swirled to dissolve the ice. Swirling was continued for about two minutes to ensure complete mixing of the two miscible liquids. The apparatus, containing the sample, was then placed into a methanol slush at approximately -98°C, causing the solution to quickly freeze. The solid was again melted until a small amount of solid, required as a seed crystal, remained. The sample was then placed into an acetone slush at about -80°C and allowed to crystallize slowly. When completely solidified, the sample was further cooled in liquid nitrogen. Further handling of the sample was done in the cold can at liquid nitrogen temperature.

In order to facilitate removal of the sample from the preparation vessel, the ground glass joint of apparatus B was allowed to warm to approximately 20°C while the sample was submerged in liquid nitrogen. Silicon lubricant was used on this joint, as well as on the stopcock. When the joint became mobile, the apparatus was quickly removed from the liquid nitrogen and lowered into the cold can so that the ball joint extended into the side arm. The stopcock was then opened to allow dry nitrogen to break the vacuum, so that the test tube could be removed at the ground glass joint. The test tube, containing the sample, was then placed into a large mortar sitting on the bottom of the cold can. Using a long-handled tool pointed at the end, the sample was removed by chipping and scraping. Long-handled spatulae were used to transfer the sample to a small screw top bottle which sat on the table. This bottle was then filled with liquid nitrogen, its top was screwed in place, and it was lowered inside a larger, nitrogen-filled, bottle. The larger bottle had a screw top attached to a piano wire so that the entire assembly could be hung in a five-liter, liquid-nitrogen, dewar for storage.

Before investigation, the sample was ground at liquid-nitrogen temperature by a Spex, Freezer-Mill, power-grinder. The usual procedure was to grind the sample for one hundred 5 sec periods allowing 30 sec for heat dissipation between the periods. This amount of grinding

produced a sufficiently fine powder to yield good spectra and powder diffraction photographs.

To prepare ammonia hemihydrate which contained 5 or 10% of deuterium, partially deuterated water was used. For example, to prepare $2NH_3 \cdot H_2O$ containing 5 mole percent of D, the ammonia, NH_3, was mixed with a stoichiometric amount (Table 2.1) of a mixture of 80 mole % of H_2O and 20 mole % of D_2O, i.e. 4 ml of H_2O to 1 ml of D_2O. To avoid dilution of the D_2O by exchange with the atmosphere, the H_2O was put into test tube A and the D_2O was syringed into it from a pre-deuterated syringe with the needle just above the liquid surface. The test tube was immediately attached to the pre-deuterated vacuum line and the water was degassed. The remaining procedure was the same as for the pure hemihydrate.

Neat deuterated-ammonia hemideuterate, $2ND_3 \cdot D_2O$, was made from stoichiometric volumes (Table 2.1) of ammonia-d_3 and deuterium oxide by the above procedure. Since the ND_3 and D_2O contained only 99 and 99.5 atom % of D, respectively, the $2ND_3 \cdot D_2O$ contained 99.12 atom % of D. $2ND_3 \cdot D_2O$ containing 5 mole % of H was prepared from ND_3 and a mixture of 20 mole % of H_2O and 80 mole % of D_2O (Table 2.1).

$2\ ^{15}NH_3 \cdot H_2O$ was made by the method used for the normal compound.

2.5 Preparation of Ammonia Monohydrate

The apparatus for the ammonia monohydrate preparation (Fig. 2.1) was the same as that used for the ammonia hemihydrate preparation. Stoichiometric volumes (Table 2.1) of ammonia and water were condensed into apparatus B, following the procedure discussed in Section 2.4. Apparatus B was removed from the vacuum line and the ice/ammonia layers were melted by warming in a slush bath at -45°C. The solution was swirled to ensure proper mixing of the two liquids. As indicated in the literature (14), crystallization proved to be difficult. Rollet and Vuillard (15,16) observed that vitrification usually occurred for dilute solutions, but crystallization could be induced by slowly warming the glass to the melting point. Thus, apparatus B, containing the homogeneous ammonia-water solution was plunged into liquid nitrogen which transformed the solution into a clear glass. The test tube containing the sample was then placed into a methanol slush at approximately -98°C and allowed to warm until the melting point was reached. As the sample warmed, the appearance of the solid changed from clear and glassy to white. Only a small amount of melting was allowed before the sample was again cooled to -98°C in the methanol slush until it was completely solid, when it was further cooled in liquid nitrogen.

Removal of the solid ammonia monohydrate from the

apparatus proved to be difficult, because the sample was very hard to break into pieces. All of the glass tubes used to prepare the monohydrate had to be broken in order to recover the sample. The sample was ground and stored in liquid nitrogen as described in Section 2.4.

2.6 Characterization of the Samples

The ammonia hydrates were characterized by X-ray powder diffraction photography. An Enraf-Nonius Diffractis 601 generator was used to produce nickel-filtered copper Kα radiation of mean wavelength 1.5418 Å (25). A Jarrel-Ash precession camera served as a flat-plate powder camera. The crystal-to-film distance was found by Bates (26) to be 59.8 mm and the usual exposure time was 8 hours with a medium collimator.

Powdered hydrate sample was loaded into a 0.5 mm (i.d.) glass capillary held upright in a small cold can. The capillary sat in a brass block with a tapered hole. The sample was added in small amounts and was packed with a fine glass rod. Once filled, the capillary was attached to a bakelite holder by means of an oil film which would freeze to the glass in approximately ten seconds. In order to transfer the capillary-and-holder assembly to the X-ray camera, tongs were used to submerge the assembly in liquid nitrogen which was contained in a metal cup with a wooden handle. At the camera, the sample was quickly transferred from the liquid nitrogen into a stream of cold

nitrogen gas and was attached securely to the goniometer head. The sample was cooled at the camera by a continuous stream of cold nitrogen gas which was carried to it from a 50 liter dewar of liquid nitrogen by a glass dewar tube. A coaxial stream of warm nitrogen gas surrounded the cold nitrogen stream to reduce condensation (27,28). Both gas streams were produced by 100 watt pencil heaters immersed in liquid nitrogen in 50 liter dewars. Variac settings of 80 V for the warm nitrogen and 100 V for the cold nitrogen produced a uniform gas flow, and a temperature of approximately -170°C measured at the sample by a copper-constantan thermocouple. The capillary was aligned perpendicular to the X-ray beam, and was rotated about its axis while the photographs were taken so that the effect of small single crystallites was reduced.

The diffraction pattern on the developed X-ray film consisted of concentric circles, the inner and outer diameters of which were measured to ±0.10 mm. This data was processed by the program POWDER, written by S. Sunder, in this laboratory. This program calculates the interplanar spacings, i.e. the d-spacings, and the diffraction angles, i.e. the 2θ values, which may be compared to literature values (3,4) for indexing and for sample identification. A parameter refinement program, DREFINE (29), was used to determine the unit cell parameters from the indexed 2θ values by a least squares fit of sin θ/λ data.

Relative intensities of the diffraction circles were measured as peak heights on microdensitometer traces of the photographs. The microdensitometer was a Joyce, Loebl and Co. Ltd. Model MK III C.

2.7 Preparation and Handling of Infrared Samples

The low-temperature infrared cell (Fig. 2.2), used to obtain infrared spectra in this work, was constructed by the Chemistry Department Machine Shop and consisted of two stainless steel sections. The inner section consisted of a liquid nitrogen reservoir closed at the bottom by the top of a copper sample holder. Cesium iodide windows, which contained the mull, fitted into the sample holder and were held in place by a spring attached to a copper ring. The spring was compressed by a faceplate which was held against the holder by four screws.

The outer section of the cell enabled the cold sample to be thermally insulated by a vacuum, and allowed the radiation to pass through two cesium iodide windows. Buna N rubber o-rings provided a vacuum seal between the windows and the outer section, as well as between the inner and outer sections of the cell when fitted together. The cell was evacuated through the nupro valve to a pressure of 10^{-2} Torr.

The temperature of the sample was controlled by cooling from the liquid nitrogen reservoir and by two heaters to which voltage was supplied by a variac. If the variac

Inner Cell'

Outer Jacket

Electrical
Feed-through

Nupro Valve

O-rings

Flange

Liquid Nitrogen
Reservoir

10 cm

Heater

Cesium Iodide
Window

O-rings
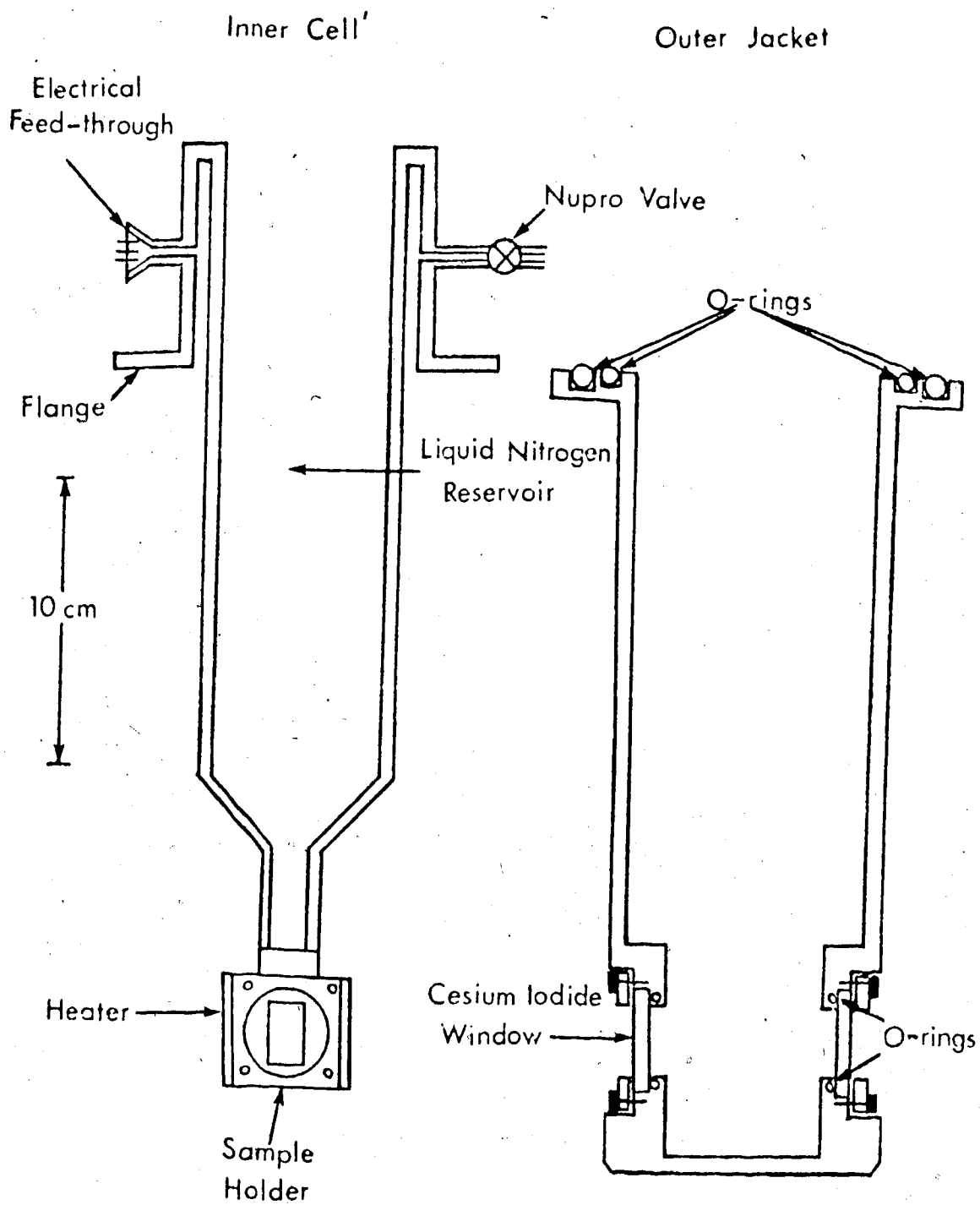
Sample
Holder

Figure 2.2   Liquid nitrogen infrared cell.

was set to 10-15 volts, the sample temperature was in the range 90-100°K. The temperature was measured by two copper-constantan thermocouples, one fastened to the top of the sample holder and one to the bottom. The voltage of the thermocouples was measured by a potentiometer and was converted to temperature by standard tables. The temperature was adjusted by the difference between the tabulated and observed voltages at 77°K. Without the heaters, the temperature of the sample dropped below the melting points of the mulling agents which are 85°K for propane, 88°K for propylene, and 92°K for chlorotrifluoromethane.

The infrared mulls were prepared in the cold can described in Section 2.3. The inner section of the cell was clamped upright in the cold can, with the sample holder resting on the back of the brass table and the flange above the top of the can. Heating tape was wrapped around the cell below the flange, but above the top of the can, to prevent condensation of ice on the cell. About 40 volts were usually applied to the heating tape. The faceplate, backed with masking tape through which four screws were pushed, was also set on the table before filling the can to just below the table top with liquid nitrogen. Once the can was filled, the cesium iodide windows on their respective holders were lowered into the can. The bottom window rested on a platform which was supported by a retort stand, which stood in the side arm of the cold can, so

that the window was just above the brass table. The top
window, which had a central indentation, rested on the
spring which was placed on the table with tweezers.
After five minutes, the sample vial was transferred to
the cold can and the screw-top was removed with tweezers.
By this time the windows were cold enough to be allowed to
contact the sample. A long spatula was used to place a small
amount of sample near the center of the bottom window and the
vial was closed and returned to its storage dewar. The mull-
ing agent (propane, propylene or chlorotrifluoromethane) was
condensed directly from a gas cylinder into a pipette which
was cooled by holding it above the level of liquid nitrogen in
the can. Drops of mulling agent from the pipette were placed.
directly on the window so that they mixed with the solid sample.
The top window was then placed on the sample. A pair of
pointed tweezers, which fitted into the indentation of the
top window, was used to rotate the top window to smear
the solid and mulling agent into a uniform mull. Tweezers
were then used to lift the windows to the sample holder
and put the spring in place against the windows. While
holding the faceplate in position with tweezers, a screw-
driver, inserted through a hole in the side of the cold
can, was used to secure the faceplate to the holder. The
retort stand which had held the windows was then removed.
The inner section of the cell, which was connected to a
vacuum line by rubber tubing and a glass ball joint, was
evacuated up to the nupro valve. The heating tape was

removed from the inner portion of the cell. The outer
section, which had been purged with dry nitrogen gas,
was lowered into the side arm of the cold can at an angle.
The inner-cell was quickly inserted into this section,
rotated to line up the cesium iodide windows, and removed
from the side arm. The nupro valve was immediately
opened and liquid nitrogen poured into the reservoir.
When the vacuum reached 6×10^{-2} Torr, the nupro valve was
closed, the rubber tubing was disconnected and the cell
was connected to the vacuum line by glass fittings. The
cell was evacuated at 1×10^{-2} Torr for at least one hour
before it was disconnected from the vacuum line and put
into the sample compartment of the interferometer. Pro-
vided that the vacuum seals had all formed correctly, it
could be left without harm in the interferometer, without
being connected to a vacuum line, for about three hours.

2.8 Infrared Instrumentation

A Nicolet 7199 Fourier Transform Infrared spectro-
meter was used to obtain the spectra presented in this
thesis. The interferometer system actually consists of
three separate Michelson interferometers; one modulates
the infrared beam, another modulates the He-Ne laser, and
the third modulates the white light. The He-Ne laser
interferometer allows the infrared interferogram to be
digitized at exact intervals of $n\lambda/2$, where n is a
specifiable integer and λ is the laser wavelength. For

this work, n was set to 2. This laser is also used to measure the moving mirror velocity, which was set at 0.90 cm sec^{-1} for all spectra obtained. The white light interferometer triggers the collection of data points. The peak of the white light interferogram, i.e. the point of zero path difference of the white light interferometer, occurs 0.3 mm before that of the infrared interferogram, and signals the electronics to start collecting data, which it does at the next zero crossing of the laser interferogram and at every n th crossing thereafter.

The moving mirror assembly is mounted on symmetrical dual air bearings and has a mass greater than 3 kg to reduce effects of external forces. The high- and low-pass electronic filters for the infrared signal were set with 3dB points at 100 Hz and 50 KHz. Normally the gain for the interferogram was set at 1 for the first 1024 data points and at 8 for the rest of the interferogram. When using the low temperature cell, the gain was increased by a factor of 4 to increase the signal. The mid-infrared spectra were obtained using a globar source with full aperture (6.3 mm diameter), a germanium-on-potassium-bromide beamsplitter, and a liquid-nitrogen-cooled mercury cadmium telluride detector.

Included in the 7199 system is a Nicolet 1180 20-bit computer. The system features a Diablo dual disk drive, composed of a permanent disk, which contained the oper-

ating software, and a removable disk for storage of spectral data. There is also a Hewlett-Packard graphic display terminal which allows the operator to view regions of spectra or interferograms and to determine plotting parameters. The results on the display screen may then be copied directly onto paper via a Zeta digital plotter.

The low temperature cell fitted snugly into a nitrogen-purged compartment with a plexiglass cover. This sample compartment was separated from the rest of the interferometer by cesium iodide windows through which the infrared beam passed. The system was originally purged by dry air but was later purged by dry nitrogen gas which removed carbon dioxide as well as removing water more efficiently. After inserting the cell into the sample compartment, the compartment was allowed to purge for at least 30 minutes before collecting data. For each sample, a minimum of two different data collections were made under identical conditions except that one collection averaged 100 interferograms while the other averaged 500. Signal-averaging 500 interferograms produced an excellent signal-to-noise ratio while averaging 100 interferograms enabled the quality of the sample to be quickly checked and indicated the reproducibility of the weak features. The interferograms were collected to give 1 cm^{-1} spectral resolution, that is,

16,384 data points were collected and 16,384 zero points were added to yield 32,768 points to be Fourier transformed. Typical values of the parameters used are given in the Appendix.

Each sample spectrum was ratioed against a background spectrum of the empty cell and was plotted as absorbance versus wavenumber from 4000 to 400 cm^{-1}. The interferometer actually yielded spectra for 8190 cm^{-1} to 0 cm^{-1} with the parameters used, but the signal levels are too low below 400 cm^{-1} and above 6000 cm^{-1} to yield useful results. The samples did not absorb sufficiently strongly to give useful spectra from 4000 to 6000 cm^{-1} which is, in any case, a region of the spectrum that was not of value to this study.

The frequency accuracy of the infrared spectrometer was checked by recording spectra of standard gases (30). It was found to be accurate to at least ±0.1 cm^{-1}.

CHAPTER III.

X-RAY POWDER DIFFRACTION PATTERNS AND MID-INFRARED SPECTRA

OF AMMONIA MONOHYDRATE AND AMMONIA HEMIHYDRATE

3.1 Introduction

This chapter describes the X-ray powder diffraction patterns and mid-infrared spectra of ammonia monohydrate and ammonia hemihydrate obtained at $95 \pm 10°K$.

Samples of $2NH_3 \cdot H_2O$, $2NH_3 \cdot H_2O$ containing 5 and 10 mole percent of D, $2ND_3 \cdot D_2O$, $2ND_3 \cdot D_2O$ containing 5 mole percent of H and $2 \, ^{15}NH_3 \cdot H_2O$ were prepared as described in Section 2.4. The preparation of $NH_3 \cdot H_2O$ is described in Section 2.5. The samples were characterized by X-ray powder diffraction photographs (Section 2.6) and the results are presented in Section 3.2. The survey spectrum of ammonia monohydrate is presented in Section 3.3 and discussed in Chapter IV. The mid-infrared spectra of ammonia hemihydrate and its isotopic forms are presented in Section 3.4 and discussed in Chapter V.

The mid-infrared spectra presented in this chapter were obtained from spectra of mulls in propane, propylene and chlorotrifluoromethane by subtraction of the absorption by the mulling agent. The subtraction was either done by the subtraction program of the Nicolet spectrometer or manually, or by a mixture of the two. The manual subtraction consists of instructing the computer to draw a straight

37

line between points on the spectrum which are chosen manually so that the straight line replaces the peak. All spectra were plotted by the Nicolet spectrometer, without smoothing, and have not been redrawn.

In the remainder of this thesis, $2NH_3 \cdot H_2O$ containing 5 mole percent of D and $2ND_3 \cdot D_2O$ containing 5 mole percent of H, etc., will be referred to for brevity as $2NH_3 \cdot H_2O$ (5% D) and $2ND_3 \cdot D_2O$ (5% H), etc. The only exception is that the purest deuterated form will simply be called $2ND_3 \cdot D_2O$ even though it actually contained 0.88 mole percent of H (Section 2.4).

3.2 Characterization of Ammonia Hemihydrate and Ammonia Monohydrate Samples

As there was doubt concerning the composition of the phases studied by Waldron and Hornig (5), it was very important in this study to characterize the samples before obtaining the infrared spectra. Possible impurities were ammonia monohydrate in the ammonia hemihydrate sample, ammonia hemihydrate in the ammonia monohydrate sample, and ice and solid ammonia. All impurities present were easily identified by the X-ray powder diffraction photographs (31,32). $NH_3 \cdot 2H_2O$ is a possible impurity, particularly in the $NH_3 \cdot H_2O$ samples, but no features were detected that could not be assigned to one of the other impurities, so no evidence of $NH_3 \cdot 2H_2O$ was found.

The X-ray data for ammonia hemihydrate and ammonia monohydrate at 100°K are summarized in Tables 3.1 and 3.2, respectively. The crystal to film distance was 59.8 mm as measured by Bates (26). The diffraction pattern of $2NH_3 \cdot H_2O$ is indexed on the standard space group Pnma (D_{2h}^{16}) (4,19). The lattice parameters were determined by the program DREFINE (29) to be a = c = 8.37 ± 0.02 Å and b = 5.31 ± 0.02 Å. These axes are 0.4% shorter than the values reported (4) at 178°K but the equality of the lengths of the a and c axes is maintained. The combined errors, however, do not permit a definite conclusion concerning the effect of temperature on the axial lengths. The diffraction pattern of $NH_3 \cdot H_2O$ is indexed on the standard space group $P2_12_12_1$ (D_2^4) (3). The lattice parameters at 100°K were found to be a = 4.51 ± 0.02 Å, b = 5.61 ± 0.02 Å and c = 9.73 ± 0.02 Å which agree well with those reported (3) for 110°K.

The diffraction patterns showed that some hemihydrate samples contained ammonia monohydrate impurity and some contained solid ammonia impurity, while some monohydrate samples contained ice and hemihydrate impurities. The effects of these impurities on the infrared spectra were easily identified by comparing the spectra of samples with different amounts of impurity.

The observed intensities of the diffraction lines that are listed in Tables 3.1 and 3.2 are the relative peak heights measured from microdensitometer traces. These

TABLE 3.1

X-Ray Powder Diffraction Pattern of

Ammonia Hemihydrate at ~100°K

Index [a]	$2\theta_{obs}$ [b]	d_{obs} [c]	I_{obs} [d]	$2\theta_{calc'd.}$ [e]	$I_{calc'd.}$ [f]
101	14.89	5.95	<5	14.97	2[†]
011	19.81	4.48	5	19.79	4
200 + 002	21.17	4.20	5	21.23	8
111	22.55	3.94	15	22.49	5
201 + 102	23.65	3.76	5	23.77	5
210	27.12	3.29	40	27.12	25
211 + 112	29.22	3.056	100	29.19	100
202	30.16	2.963	10	30.20	9
020 }	33.89	2.645	50	33.74	N.S.F.
103 + 301				33.87	19
212			<1	34.70	2
013	36.38	2.469	20	36.37	22
121			<5	37.10	0.12[†]
113 + 311	37.94	2.371	15	37.98	17
203 + 302	38.80	2.321	20	38.80	20
220 + 022	40.13	2.247	<5	40.21	1
122 + 221			<2	41.69	1

Table 3.1, continued

Index[a]	$2\theta_{obs}$[b]	d_{obs}[c]	I_{obs}[d]	$2\theta_{calc'd.}$[e]	$I_{calc'd.}$[f]
213 + 312	42.50	2.127	5	42.50	10
400 + 004	43.31	2.089	5	43.24	6
104 + 401	44.52*	2.035	<2	44.64	2
222 + 303	45.95	1.975	~2	45.91,46.01	5
410			<1	46.66	1
411 + 114			<1	47.98	<1
123 + 321	} 48.62*	1.873	~2	48.56 }	6
402 + 204				48.65	

[a] Indexed on the standard space group Pnma (D_{2h}^{16}).

[b] CuKα radiation, $\lambda = 1.5418$ Å. Precision $\pm 0.1°$. The starred values were not used to calculate lattice parameters.

[c] Precision ± 0.04 Å at small angles to ± 0.004 Å at large angles.

[d] Relative peak heights on microdensitometer traces.

[e] Using the values $a = 8.37$ $b = 5.31$ $c = 8.37$, all ± 0.02 Å, determined by refinement to the unstarred values of 2θ using the program DREFINE.

[f] Using the observed structure factors of Ref. 4 , and the equation given in Ref. 33. Entries marked ǂ were calculated from the calculated structure factors of Ref. 4 . N.S.F. means that no structure factor was reported.

TABLE 3.2

X-Ray Powder Diffraction Pattern of

Ammonia Monohydrate at ~100°K

Index[a]	$2\theta_{obs}$[b]	d_{obs}[c]	I_{obs}[d]	$2\theta_{calc'd.}$[e]	$I_{calc'd.}$[f]
002	18.08	4.91	35	18.24	40
011				18.26	
101			< 5	21.71	0.5
012	24.04	3.70	20	24.22	10
110	25.23	3.53	40	25.33	40
102	26.85	3.32	100	26.95	100
111				26.96	
112				31.39	46
013	31.60*	2.831	90	31.87	61
020				31.91	
021	33.40	2.683	~5	33.25	1.6
103			< 2	34.04	<0.1
004	36.93	2.434	10	36.96	10
022				37.00	
113				37.73	1.3
120			< 2	37.77	
121	38.88	2.316	30	38.93	34
200	39.98	2.255	20	39.95	N.S.F.
014			< 2	40.42	0.1
201			< 2	41.06	0.2

Table 3.2, continued

Index[a]	$2\theta_{obs}$[b]	d_{obs}[c]	I_{obs}[d]	$2\theta_{calc'd.}$[e]	$I_{calc'd.}$[f]
104				42.21	
	42.22	2.140	20		22
122				42.24	
023			<2	42.62	0.8
210			<2	43.22	<0.1
202			<5	44.25	
					5
211				44.26	
114	45.36	2.000	~5	45.33	11
212			<2	47.27	0.7
123	47.40	1.918	~5	47.35	6

[a] Indexed on the standard space group $P2_12_12_1$, (D_2^4).

[b] CuKα radiation, λ = 1.5418 Å. Precision ±0.1°. The starred values were not used to calculate lattice parameters.

[c] Precision ±0.04 Å at small angles to ±0.004 Å at large angles.

[d] Relative peak heights on microdensitometer traces.

[e] Using the values a = 4.51 Å b = 5.61 Å c = 9.73 Å, all ±0.02 Å, determined by refinement to the unstarred values of 2θ using the program DREFINE.

[f] Using the observed structure factors from Ref. 3 N.S.F. means that no structure factor was reported.

intensities compare well with those calculated from the
formula (33):

$$I \propto [(1+\cos^2 2\theta) / (\sin^2 \theta \cos \theta)] \cos 2\theta\ pF^2 \qquad (1)$$

where F is the observed structure factor, obtained from
Siemons and Templeton (4) for the hemihydrate and from
Olovsson and Templeton (3) for the monohydrate, and p is
the multiplicity factor (33).

The agreement shown in Tables 3.1 and 3.2 between the
observed X-ray powder diffraction patterns and those cal-
culated from the data of the single crystal studies (3,4)
leaves no room for doubt that the samples studied were the
desired compounds.

3.3 Mid-Infrared Spectra of $NH_3 \cdot H_2O$

The mid-infrared spectrum of $NH_3 \cdot H_2O$ at ~95°K is
shown in Figure 3.1 and the frequencies of the spectral
features are listed in Table 3.3. The mulling agent ab-
sorption has been accurately subtracted, except near
2900 cm^{-1} and 1500 cm^{-1} where straight lines appear in
curve A. The absorption by the propane mulling agent was
too intense at these frequencies to be reliably subtracted.
Spectra obtained from mulls in chlorotrifluoromethane
(Curves B and C of Figure 3.1) clearly show the features
present in these regions. Figures 3.2 to 3.4 show the
important regions of absorption, 3700 to 2700 cm^{-1}, 1950
to 1360 cm^{-1} and 1200 to 600 cm^{-1}, on expanded scales.
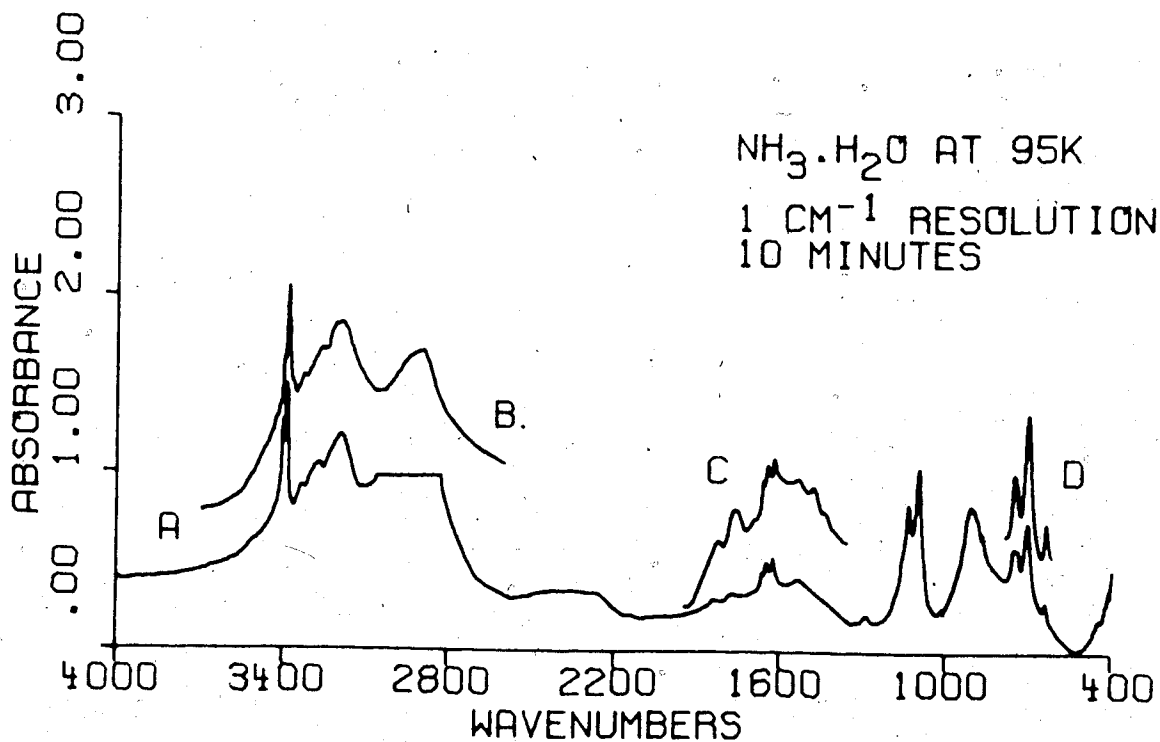
Figure 3.1 Mid-infrared spectrum of $NH_3 \cdot H_2O$ at ~95°K; 1 cm^{-1} resolution. The lettered curves were obtained from different samples and are offset for clarity. In Curve A, straight lines appear where absorption by the mulling agent was too strong to subtract accurately.

TABLE 3.3

Frequencies of Features Observed in

the Mid-Infrared Spectra of Ammonia

Monohydrate at ~95°K

$NH_3 \cdot H_2O$			$^{15}NH_3 \cdot H_2O$
ν^a/cm^{-1}	Intensity	Assignment[b]	$\nu^{a,c}/cm^{-1}$
3402(2)	vs	$\left.\begin{array}{c} \\ \nu_3(NH_3) \\ \\ \end{array}\right\}$	3396(1)
			3384(1)
3387(2)	vs		3380 sh
3330(3)	s	$\left.\begin{array}{c} 2\nu_4(NH_3) \\ + \\ \nu_1(NH_3) \end{array}\right\}$	
3305(2)	sh		
3287(2)	sh		
3270(5)	s		
3190(10)	vs	ν (O-H···O)	
2910(10)	vs	ν (O-H···N)	
2500-2250	w,vbr	o/c	
2142(2)	vw	o/c	
~2025	vw,br	o/c	
1833(5)	w	o/c	
1770(5)	w	o/c	
~1700	sh	o/c	
1664(1)	mw	$\left.\begin{array}{c} \\ \nu_4(NH_3) \\ \end{array}\right\}$	1661(1)
1650(2)	mw		1648(1)
1625(2)	mw		1624(1)

Table 3.3, continued

NH$_3$·H$_2$O			^{15}NH$_3$·H$_2$O
ν^a/cm^{-1}	Intensity	Assignment^b	$\nu^{a,c}$/cm^{-1}
1540(5)	w	ν_2(H$_2$O)	
1483(5)	w	o/c	
1440(5)	sh	o/c	
1287(2)	vw	o/c	
1133(2)	ms	ν_2(NH$_3$)	1129(2)
1095(2)	s		d
908(3)	ms		908(3)
895(2)	ms	ν_R	897(2)
884(2)	sh		886(2)
757(2)	m		
747	sh		
708(2)	ms		708(2)
641(2)	w	ν_R	641(2)
448(2)	w		
<400			

^{a}The estimated accuracy of the frequencies is in brackets.

^{b}o/c means overtone or combination band.

^{c}Only frequencies which could be definitively measured are listed.

^{d}Masked by 2 ^{15}NH$_3$·H$_2$O absorption.
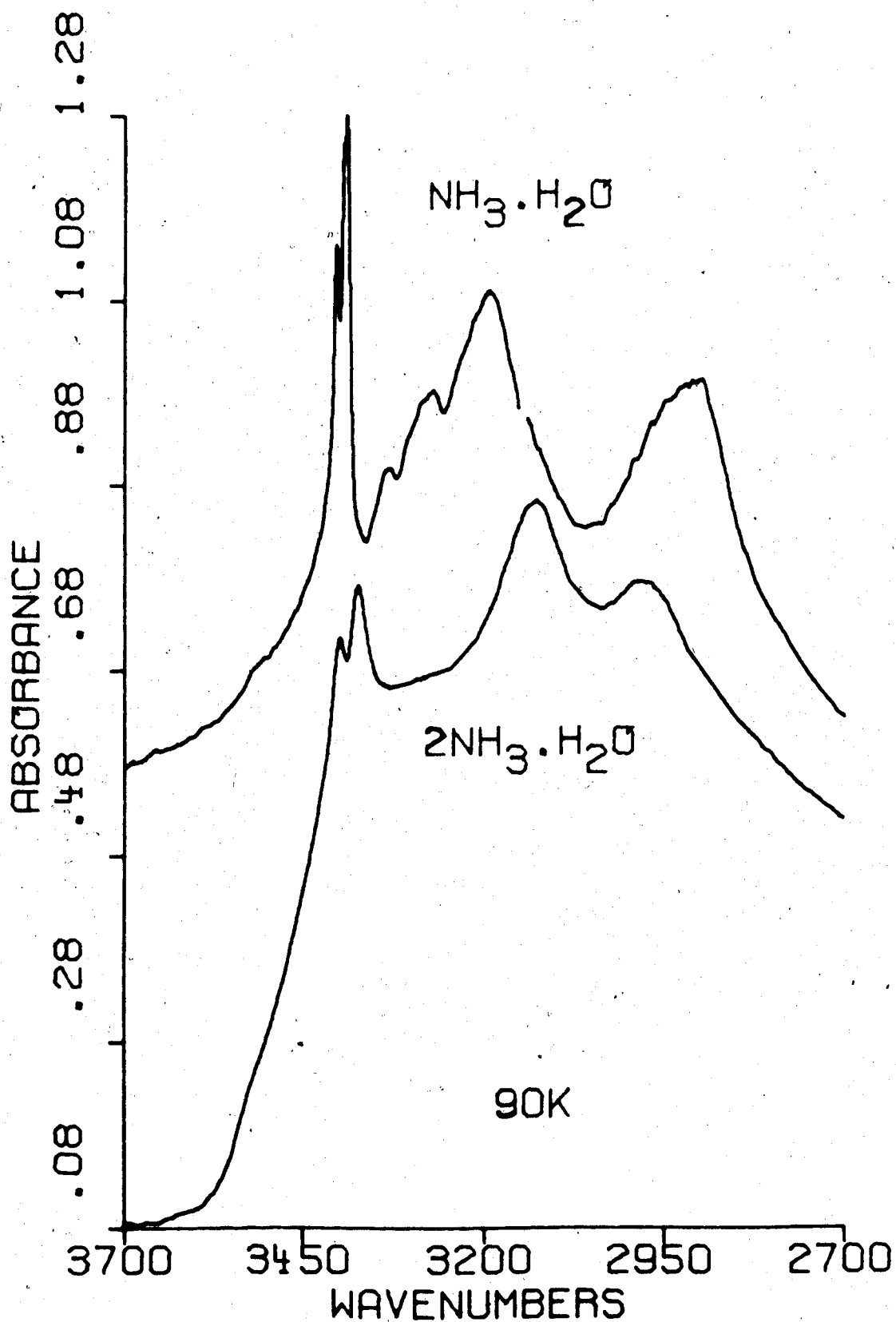
Figure 3.2 The ν(N-H) and ν(O-H) region of the spectra of
$NH_3 \cdot H_2O$ and $2NH_3 \cdot H_2O$ at ~90°K; 1 cm^{-1} resolution. The
upper curve is from two spectra of $NH_3 \cdot H_2O$, and the region
above 3150 cm^{-1} shows very little noise while the region
below 3140 cm^{-1} is noisier.
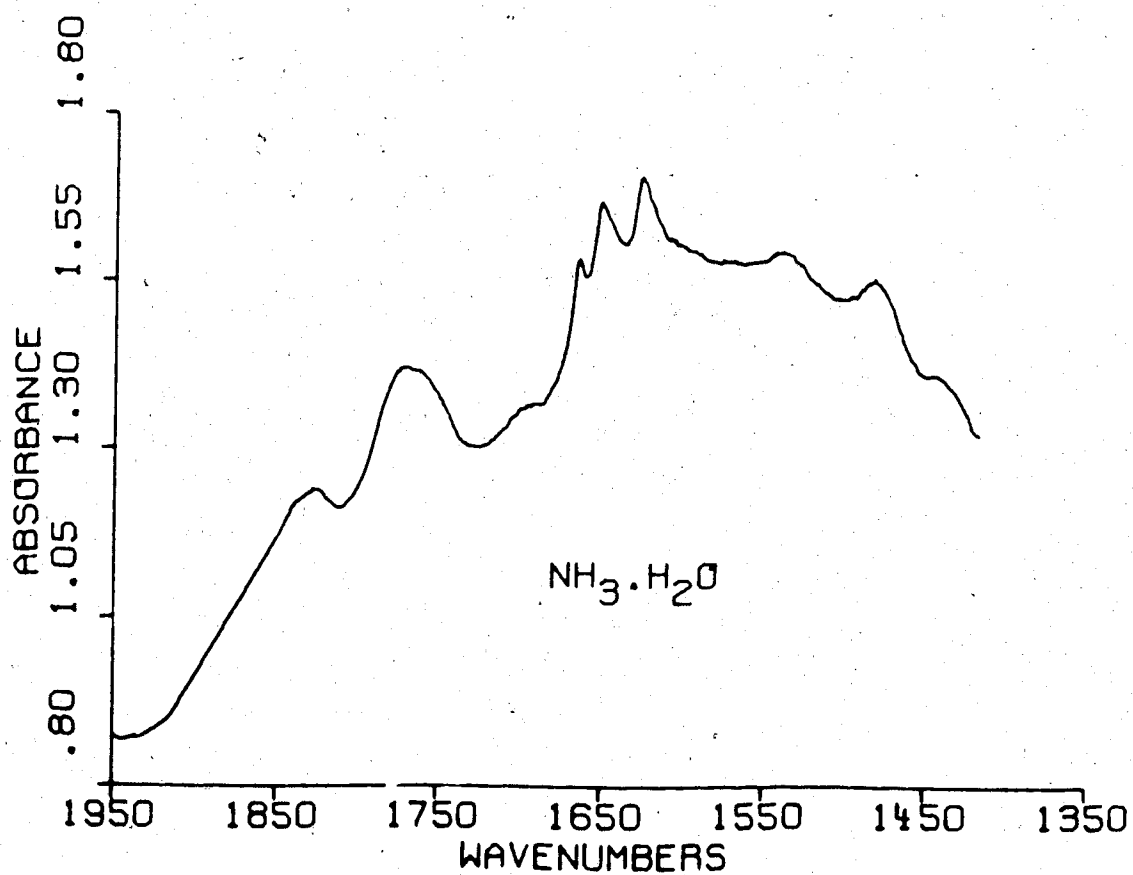
Figure 3.3 The $\nu_4(NH_3)$ and $\nu_2(H_2O)$ region of the spectrum of $NH_3 \cdot H_2O$ at $\sim95°K$; 1 cm^{-1} resolution. The notations of the vibrations are discussed in Chapter IV.
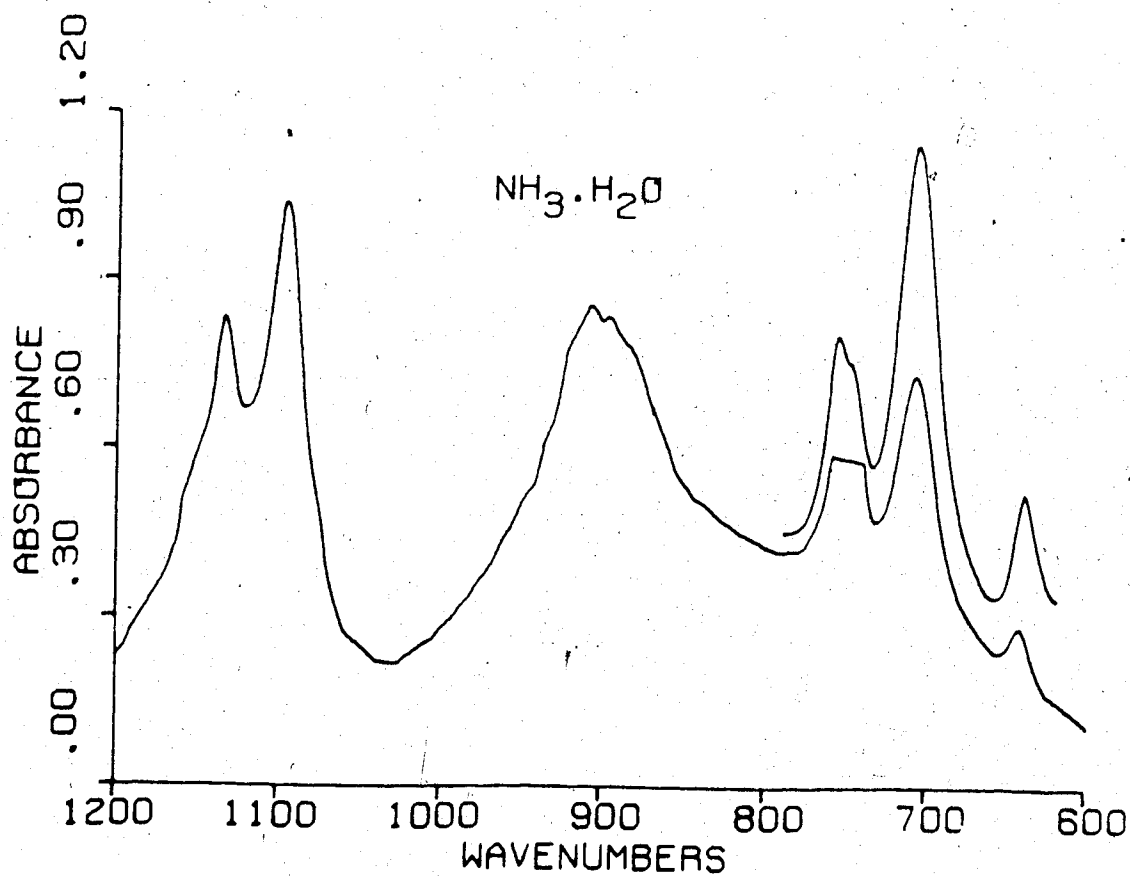
Figure 3.4   The $\nu_2(NH_3)$, $\nu_R(H_2O)$ and $\nu_R(NH_3)$ region of the spectrum of $NH_3 \cdot H_2O$ at ~95°K; 1 cm^{-1} resolution.   The superimposed curve is from a different sample and is off-set for clarity.   The shoulder at 1160 cm^{-1} is spurious. The notations of the vibrations are discussed in Chapter IV.

The only uncertainty in the spectra is the relative intensity of the two high frequency peaks near 3400 cm^{-1} (Curves A and B in Figure 3.1) which varied from spectrum to spectrum. The shoulder at 1160 cm^{-1} (Curve A of Figure 3.1 and Figure 3.4) is not a real feature but results from the subtraction of the mulling agent.

In the preparation of 2 $^{15}NH_3 \cdot H_2O$, a significant amount of $^{15}NH_3 \cdot H_2O$ impurity was obtained. As a result, frequencies of features due to $^{15}NH_3 \cdot H_2O$ were measured. Frequencies which could be definitively measured are listed in Table 3.3. The features due to $^{15}NH_3 \cdot H_2O$ could be identified without doubt since spectra of samples containing different amounts of impurity were obtained.

The spectrum of $^{15}NH_3 \cdot H_2O$ clearly shows a triplet in the high frequency region, namely two sharp peaks at 3396 and 3384 cm^{-1} and a shoulder at 3380 cm^{-1}. The spectrum of $^{14}NH_3 \cdot H_2O$ shows with certainty only a doublet at 3402/3387 cm^{-1}.

3.4 Mid-Infrared Spectra of $2NH_3 \cdot H_2O$

The mid-infrared spectrum of $2NH_3 \cdot H_2O$ at ~95°K is shown in Figure 3.5 while the frequencies of the spectral features are listed in Table 3.4. The mulling agent absorption has been subtracted, except near 2900 and 1500 cm^{-1} in curve A, where it was too intense. Straight lines appear in these regions.

Only two uncertainties in the spectra presented are
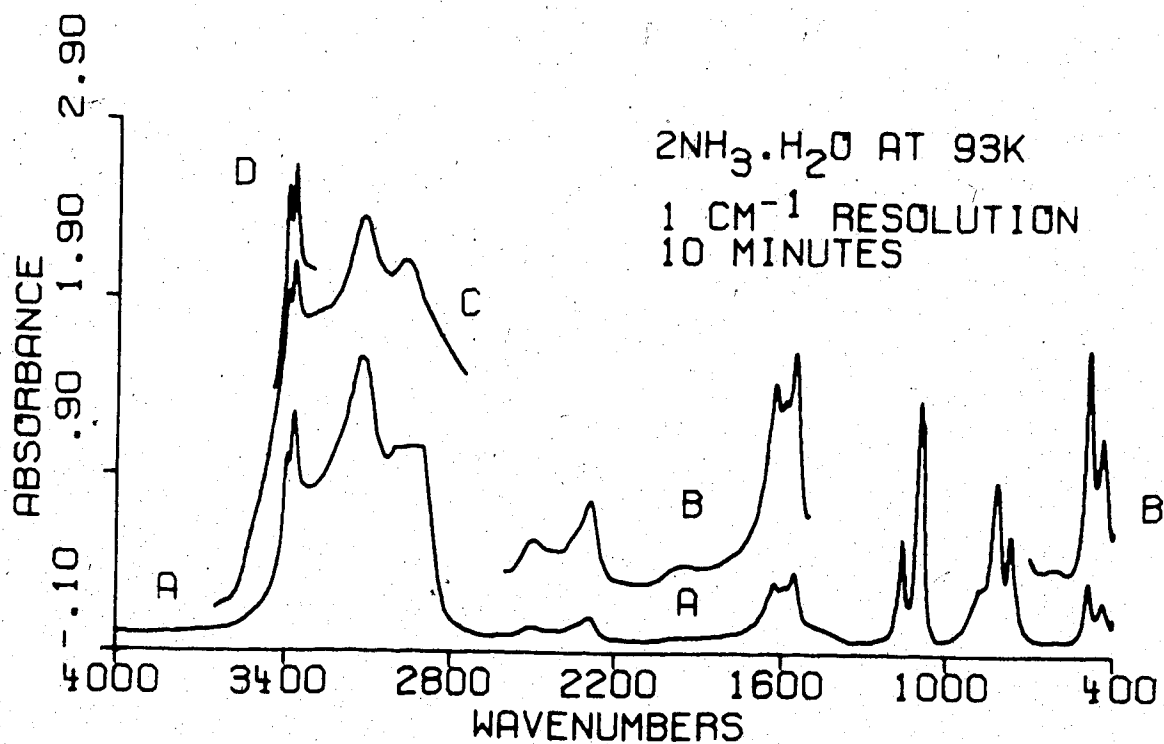
Figure 3.5 Mid-infrared spectrum of $2NH_3 \cdot H_2O$ at ~95°K; 1 cm^{-1} resolution. Curves labelled with different letters were obtained from different samples and are offset for clarity. Straight lines near 2900 and 1500 cm^{-1} in curve A indicate regions where the mulling agent absorption was too intense to be subtracted.

TABLE 3.4

Frequencies of Features Observed in

the Mid-Infrared Spectra of Ammonia

Hemihydrate at ~95°K

$2NH_3 \cdot H_2O$			$2\ ^{15}NH_3 \cdot H_2O$
ν^a/cm^{-1}	Intensity	Assignment[b]	$\nu^{a,c}/cm^{-1}$
3397(2)	s	ν_3 (NH_3)	d
3374(2)	vs		3366(2)
3125(10)	vs	$\nu_{OH \cdots N}$	3130(10)
2975(10)	vs	$\nu_{OH \cdots N}$	2975(10)
2500(4)	mw	o/c	
~2350	sh	o/c	
2294(2)	mw	o/c	
2180(2)	vw	o/c	
2120(2)	vw	o/c	
~1950	vw,br	o/c	
~1790	br,sh	o/c	
1626(2)	m	ν_2 (H_2O)	d
1590(2)	m	+	d
1555(1)	m	ν_4 (NH_3)	1554(4)
1156(2)	ms		1154(2)
1092(2)	vs	ν_2 (NH_3)	1088(2)
1083(2)	vs		1076(2) sh

Table 3.4, continued

2NH$_3$·H$_2$O			2 ^{15}NH$_3$·H$_2$O
ν^a/cm^{-1}	Intensity	Assignment^b	$\nu^{a,c}$/cm^{-1}
~882	sh	ν_R (H$_2$O)	
817(2)	s		817(3)
767(2)	ms		765(2)
~610	vw,br	ν_R (NH$_3$)	
489(1)	m		489(1)
441(1)	m		441(4)

^{a}The estimated accuracy of the frequencies is in brackets.

^{b}o/c means overtone or combination band.

^{c}Only frequencies which could be definitively measured are listed.

^{d}Masked by ^{15}NH$_3$·H$_2$O absorption.

known. The relative intensities of the doublet near 3400 cm^{-1} (Curves A, C and D) varied significantly from sample to sample and are, thus, uncertain. It is obvious that no strong features are present in the 1522 to 1360 cm^{-1} region of the spectrum (Curve A), although the existence of weak features is uncertain.

Spectral regions of $2NH_3 \cdot H_2O$ (5% D) and $2NH_3 \cdot H_2O$ (10% D) which differ from those of $2NH_3 \cdot H_2O$ are presented in Figures 3.6 to 3.8. Spectra of $2ND_3 \cdot D_2O$ and the spectral regions of $2ND_3 \cdot D_2O$ (5% H) which differ from those of $2ND_3 \cdot D_2O$ are presented in Figures 3.9 to 3.11. Frequencies corresponding to the features in these spectra are listed in Tables 3.5 to 3.7.

The lower plot in Figure 3.6 shows the 2550 to 1950 cm^{-1} region of the spectra of $2NH_3 \cdot H_2O$, $2NH_3 \cdot H_2O$ (5% D) and $2NH_3 \cdot H_2O$ (10% D). Mulling agent absorption has been subtracted in each case, except that the very weak feature in the 5 and 10% D curves at ~2378 cm^{-1} is a residual mulling agent peak. Some features were observed in the spectrum of $2NH_3 \cdot H_2O$ (5% D) but not in that of $2NH_3 \cdot H_2O$ (10% D), namely the weak peak at 2461 cm^{-1} and the 2425 cm^{-1} shoulder. Features which became more intense with increased concentration of deuterium are designated in Table 3.5 with the letter 'b'. The relative intensity of the doublet at 2445/2432 cm^{-1} varied from sample to sample (Figure 3.6, upper plot). The existence of some very weak fea-
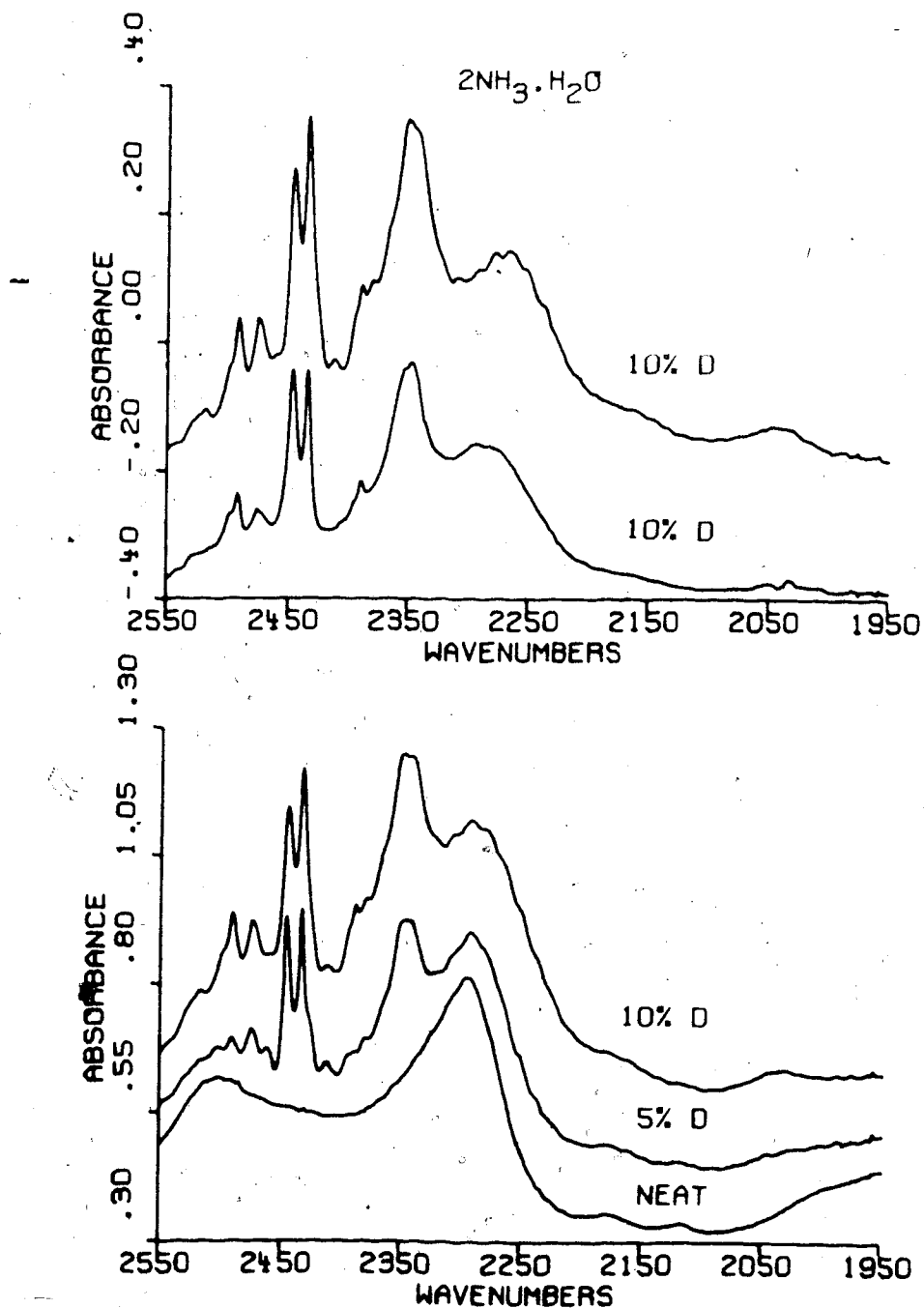
Figure 3.6 Lower plot: The absorption by $2NH_3 \cdot H_2O$, $2NH_3 \cdot H_2O$ (5% D) and $2NH_3 \cdot H_2O$ (10% D) in the $\nu(N-D)$ and $\nu(O-D)$ stretching region. Upper plot: The absorption by two different samples of $2NH_3 \cdot H_2O$ (10% D) from which the absorption by neat $2NH_3 \cdot H_2O$ has been subtracted. Sample temperature ~95°K; resolution 1 cm^{-1}. The curves are offset, and plotted with different absorbance scales, for clarity.
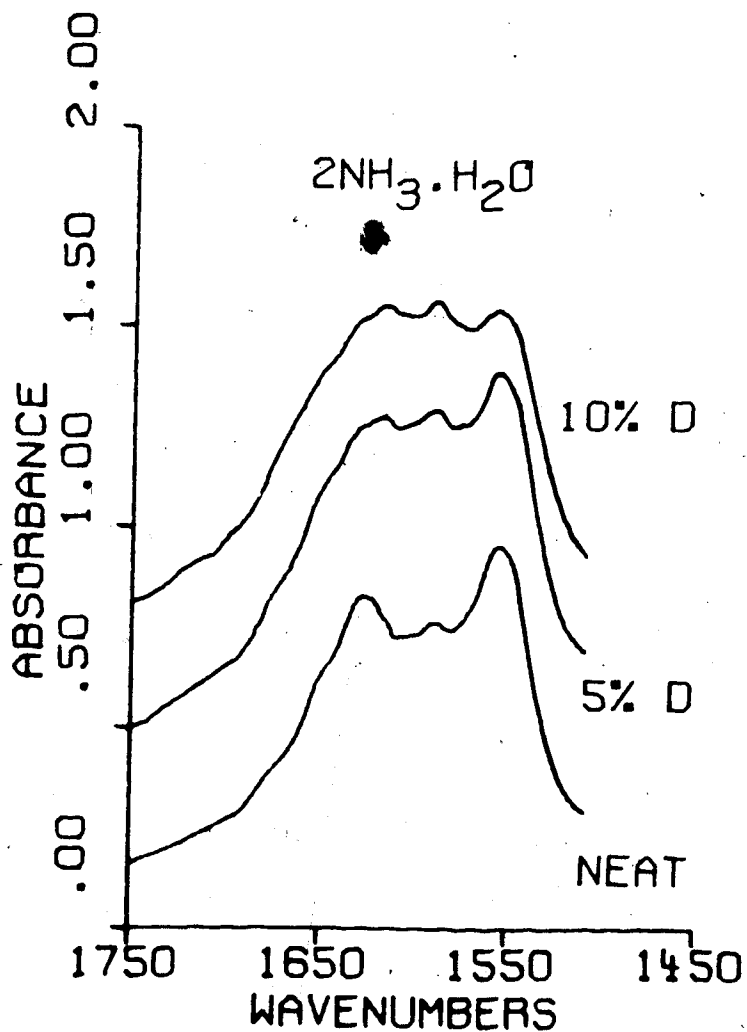
Figure 3.7 The $\nu_2(H_2O)$ and $\nu_4(NH_3)$ region of the spectra of $2NH_3 \cdot H_2O$ (5% D) and $2NH_3 \cdot H_2O$ (10% D). The curves are offset for clarity. Sample temperature ~95°K; resolution 1 cm⁻¹. The notations of the vibrations are discussed in Chapter V.
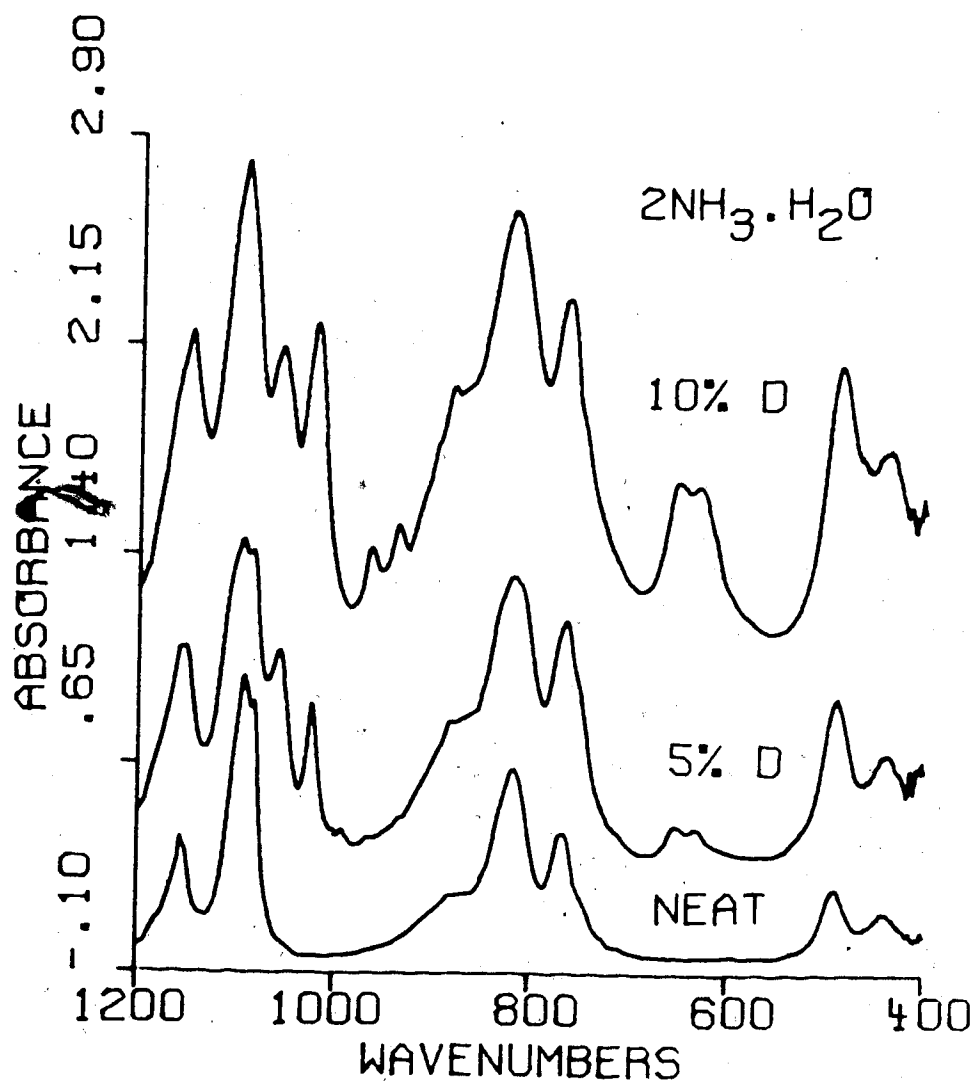
Figure 3.8 The $\nu_2(NH_3)$, $\nu_R(H_2O)$ and $\nu_R(NH_3)$ region of the spectra of $2NH_3 \cdot H_2O$, $2NH_3 \cdot H_2O$ (5% D) and $2NH_3 \cdot H_2O$ (10% D). The curves are offset, and plotted with different absorbance scales, for clarity. Sample temperature ~95°K, resolution 1 cm⁻¹. The notations of the vibrations are discussed in Chapter V.
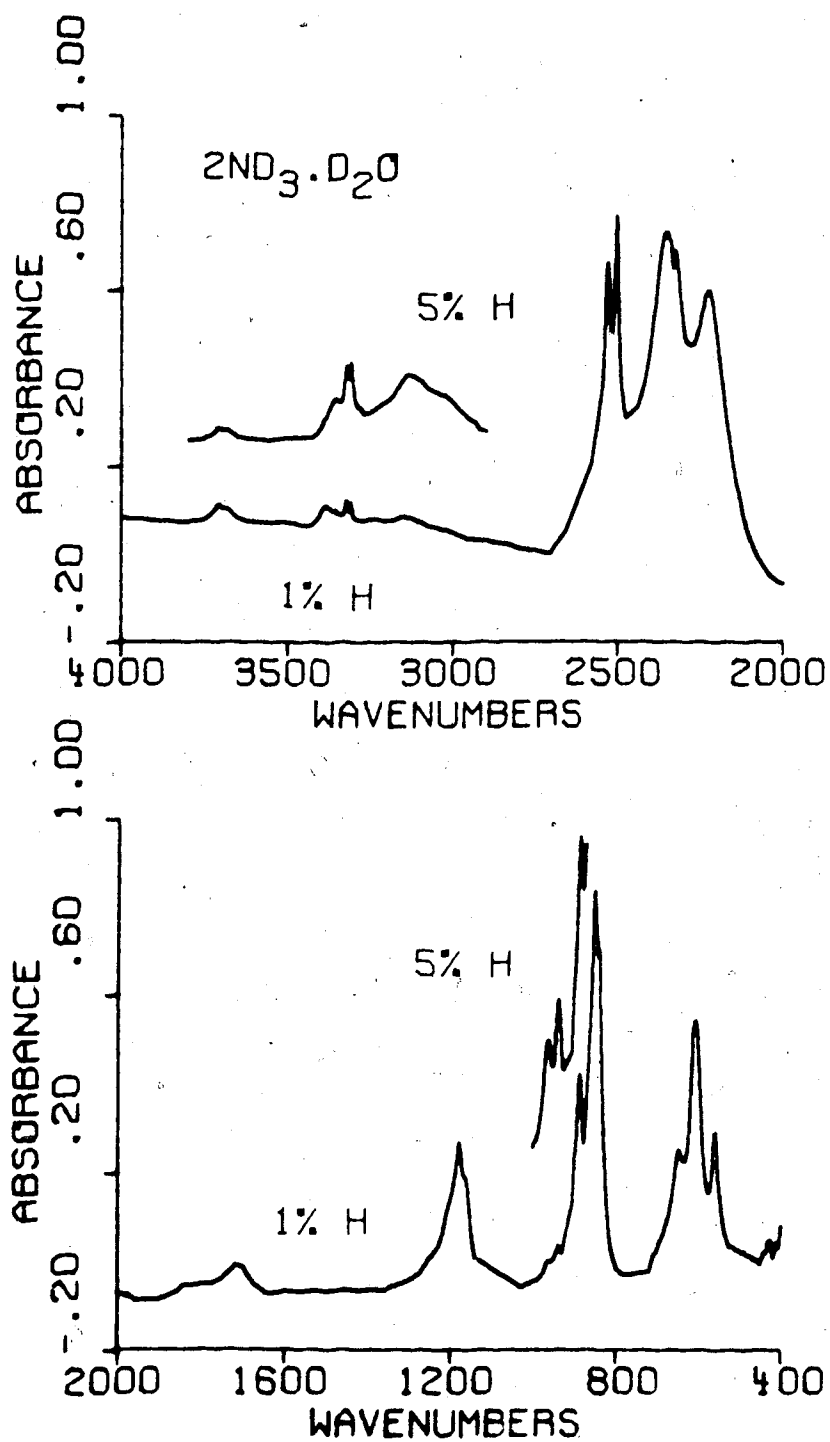
Figure 3.9 Mid-infrared spectra of $2ND_3 \cdot D_2O$ and $2ND_3 \cdot D_2O$ (5% H). The curves are offset for clarity. Sample temperature ~95°K; resolution 1 cm^{-1}.
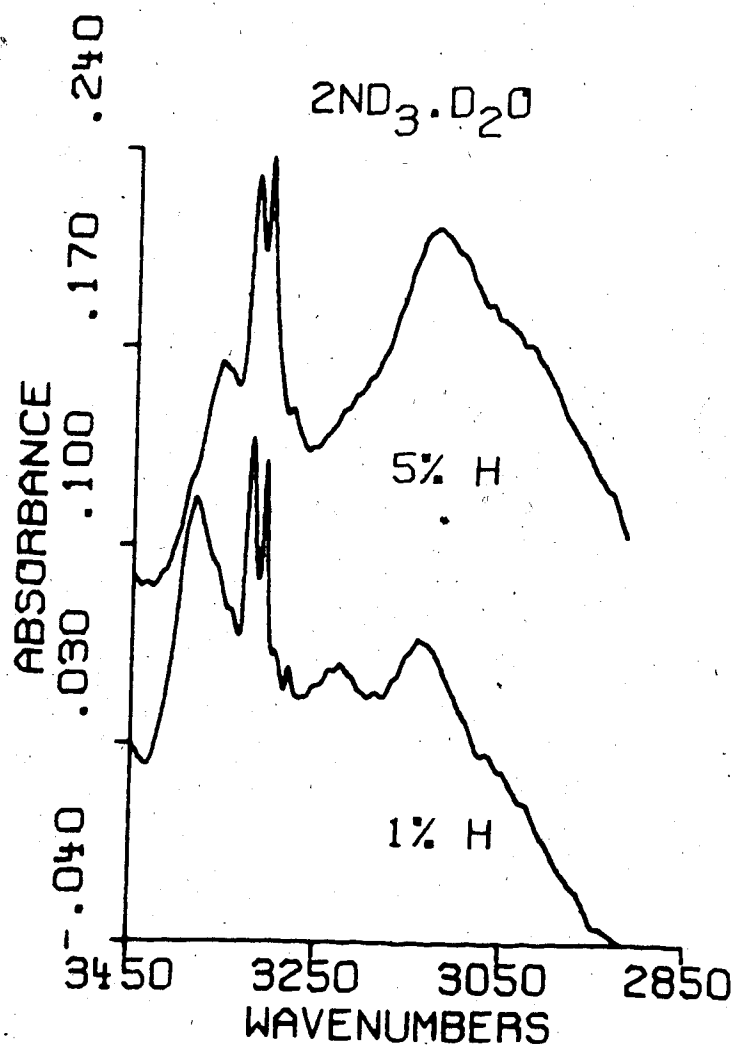
Figure 3.10   The isolated ν(N-H) and ν(O-H) region of the
spectra of $2ND_3 \cdot D_2O$ and $2ND_3 \cdot D_2O$ (5% H).   The curves are
offset, and plotted with different absorbance scales,
for clarity.   Sample temperature ~95°K; resolution $1 \, cm^{-1}$.
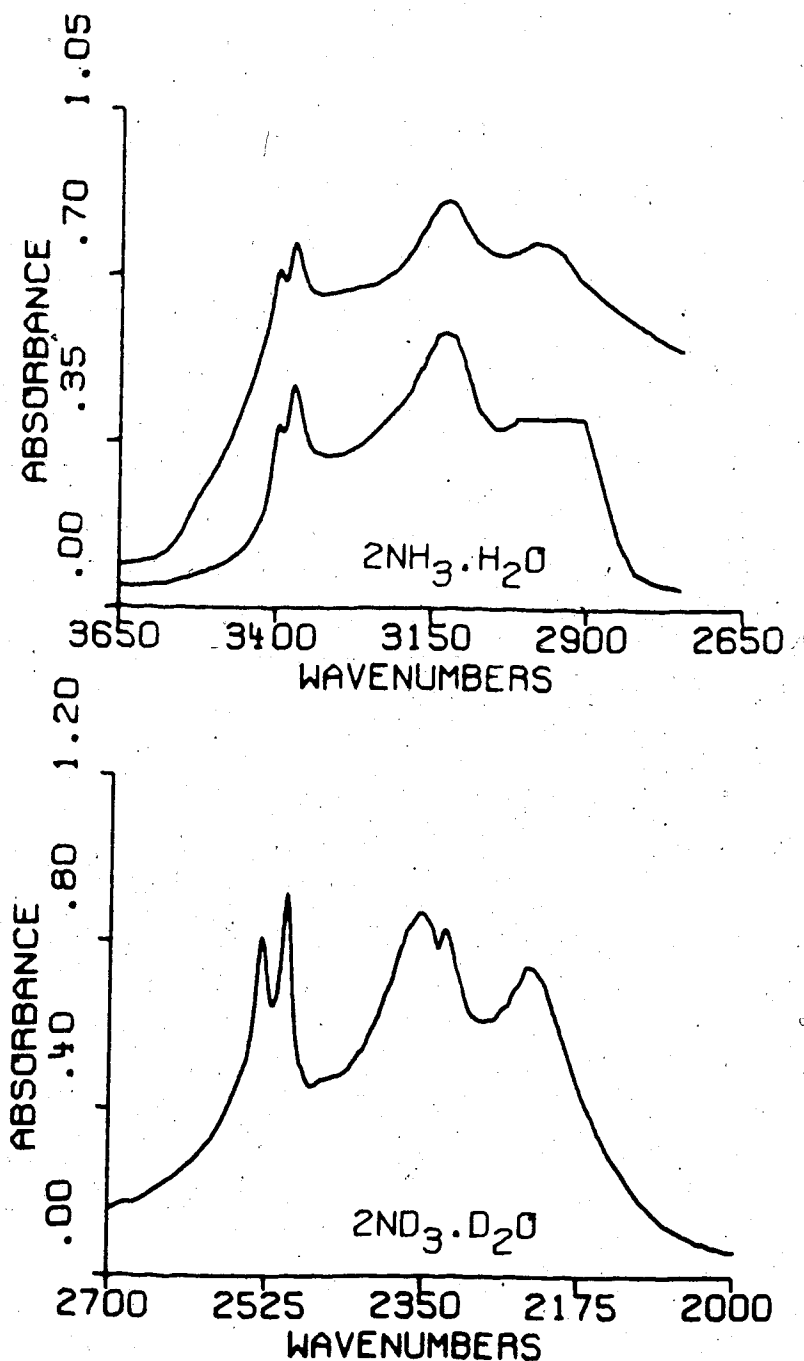
Figure 3.11   The ν(N-D) and ν(O-D) spectral region of
2ND$_3$·D$_2$O is presented in the lower plot.   The ν(N-H) and
ν(O-H) spectral region of 2NH$_3$·H$_2$O is presented in the
upper plot.   The curves in the upper plot are offset for
clarity and the low-frequency end of the upper curve is
distorted by reflection effects.   Sample temperature
~95°K; resolution 1 cm^{-1}.

TABLE 3.5

Frequencies of the Mid-Infrared Spectral
Features of Ammonia Hemihydrate Containing
5 and 10 mole % of D at ~95°K

$2NH_3 \cdot H_2O$, 5% D		$2NH_3 \cdot H_2O$, 10%D		
ν^d/cm^{-1}	Intensity	ν^d/cm^{-1}	Intensity	Assignment[e]
3397(2)	s	a		$\nu_3 (NH_3)$
3374(2)	vs	a		
3125(10)	vs	a		$\nu_{OH \cdots N} (H_2O)$
2975(10)	vs	a		$\nu_{OH \cdots N} (H_2O)$
2501(2)	vw	2498	sh	
2490(2)	w	a	b	
2473(2)	w	a	b	$\nu_{N-D} (NDH_2)$
2461(2)	vw	-		
2445(2)	m	a	b	
2432(2)	m	a	b	
2425	sh	-		
2347(4)	m	a	b	$\nu_{OD \cdots N} (HDO)$
2290(5)	m	a	b	$\nu_{OD \cdots N} (HDO)$
~2170	vw,br,sh	~2160	vw,br,sh	
2120	vw,br,sh			
~2040	vw,br,sh	~2040	vw,br	
~1950	vw,br	c		
~1790	br,sh	c		

Table 3.5, continued

$2NH_3 \cdot H_2O$, 5% D		$2NH_3 \cdot H_2O$, 10% D		
ν^d/cm^{-1}	Intensity	ν^d/cm^{-1}	Intensity	Assignment[e]
1630	sh	1630	sh	$\nu_4(NH_3)$ + $\nu_2(H_2O)$
1620(3)	m	1616(3)	m[b]	
1590(2)	m	1590(4)	m	
1555(1)	m	1555(2)	m	
1154(2)	ms	a		$\nu_2(NH_3)$
1092(2)	s	a		
1083(2)	sh			
1056(3)	ms	a		$\nu_2(NH_2D)$
1021(2)	m	1021(2)	ms[b]	
993(2)	vw			
964(2)	vw	964(2)	w[b]	$\nu_2(ND_2H)$
936(2)	vw	936(2)	w[b]	
~882	sh	a		$\nu_R(H_2O)$
817(2)	s	a		
765(2)	ms	a		
650(2)	w	650(2)	m[b]	$\nu_R(HDO)$
630(2)	w	630(2)	m[b]	
489(1)	m	a		$\nu_R(NH_3)$
441(1)	m	a		

[a] As for 5% D.

[b] This feature's intensity increases with deuterium concentration.

[c] Not studied.

[d] The estimated accuracy of the frequencies is in brackets.

[e] o/c means overtone or combination band.

TABLE 3.6

Isolated N-D and O-D Stretching Frequencies

After Subtraction of the Absorption by

the Neat Hemihydrate

$2NH_3 \cdot H_2O$, 5%D		$2NH_3 \cdot H_2O$, 10%D	
ν^a/cm^{-1}	Intensity	ν^a/cm^{-1}	Intensity
2503(3)	vw	2498	sh
2492(2)	w	2492(2)	w
2474(2)	w	2474(2)	w
2461(2)	vw		
2446(1)	m	2446(1)	m
2434(1)	m	2434(1)	m
2425	sh		
2347(4)	m	2347(4)	m
2275(15)	m	2275(15)	m
~2160	br,sh	~2160	br,sh
~2040	vw,br	~2040	vw,br

[a]The estimated accuracy of the frequencies is in brackets.

TABLE 3.7

Frequencies of the Mid-Infrared Spectral

Features of Neat Deuterated-Ammonia

Hemideuterate and the Hemideuterate

containing 5 mole % of H at ~95°K

$2ND_3 \cdot D_2O$		$2ND_3 \cdot D_2O$, 5%H		
ν^d/cm^{-1}	Intensity	ν^d/cm^{-1}	Intensity	Assignment[e]
3710(3)	w,br	c		
3685(5)	w,sh	c		
3385(5)	w,br	3385	w,sh	
3360	w,sh	3355(5)	w[b]	ν_{N-H} (ND$_2$H)
3322(2)	w	a	b	
3308(2)	w	a	b	
3282(2)	vw	a	b	
3230(5)	w,br	~3225	vw,sh	
3140(5)	w,br	3125(5)	w,br[b]	$\nu_{OH \cdots N}$ (HDO)
~3050	br,sh	a	w[b]	$\nu_{OH \cdots N}$ (HDO)
2530(2)	s	a		ν_3 (ND$_3$)
2502(2)	vs	a		
2355(5)	vs	a		$\nu_{OD \cdots N}$ (D$_2$O)
2326(2)	vs	a		
~2265	sh	a		
~2250	sh	a		
2230(2)	s	a		$\nu_{OD \cdots N}$ (D$_2$O)

Table 3.7, continued

ν^{a}/cm^{-1}	Intensity	ν^{d}/cm^{-1}	Intensity	Assignment[e]
~1840	w,br,sh	a		o/c
1705(5)	w,br	a		o/c
~1250	w,br,sh	a		
~1210	sh	a		ν_2 (D_2O)
1182(2)	m	a		+
~1160	m,sh	a		ν_4 (ND_3)
962(2)	sh	a	m[b]	
936(2)	sh	a	m[b]	ν_2 (ND_2H)
884(3)	ms	a		
848(2)	vs	a		ν_2 (ND_3)
838(2)	vs	a		
646(2)	m	a		
606(2)	ms	a		ν_R (D_2O)
560(2)	m	a		
~500	vw,br,sh	a		

where the table column groups are "$2ND_3\cdot D_2O$" (first two columns) and "$2ND_3\cdot D_2O$, 5%H" (remaining columns).

[a] As for neat $2ND_3\cdot D_2O$ (~0.8% H).

[b] This feature's intensity increases with hydrogen concentration.

[c] Not studied.

[d] The estimated accuracy of the frequencies is in brackets.

[e] o/c means overtone or combination band.

tures such as those at 2530, 2520, 2412, 2395 and 2388 cm^{-1} and the ripple on the peak near 2275 cm^{-1} is uncertain. Table 3.5 lists the frequencies of all of the features whose existence is believed to be certain.

The upper plot in Figure 3.6 presents spectra of two samples of $2NH_3 \cdot H_2O$ (10% D) after the spectrum of neat ammonia hemihydrate has been subtracted from each of them. The effect of this subtraction can be seen by comparing with the top curve in the lower plot of Figure 3.6. The most notable influence is near 2270 cm^{-1}. The lower curve of the upper plot was obtained from a mull in propylene while the upper curve was obtained from a mull in propane. The absorption by the appropriate mulling agent has been subtracted from each spectrum. This figure, thus, shows the reproducibility in these spectra of the weak absorption left after two different spectral subtractions have been made. The frequencies of the features in this plot as well as those obtained from a similar treatment of the 5% D case are presented in Table 3.6.

Figures 3.7 and 3.8 present the 1750 to 1510 cm^{-1} and the 1200 to 400 cm^{-1} regions of the spectra of $2NH_3 \cdot H_2O$, $2NH_3 \cdot H_2O$ (5% D) and $2NH_3 \cdot H_2O$ (10% D). The frequencies of the features in these spectra are listed in Tables 3.4 and 3.5. Several features are identical in all three spectra but the features in the spectra of the partially deuterated samples at 1056, 1021, 993, 964, 936, 650 and 630 cm^{-1} are not in the spectrum of neat ammonia

hemihydrate. Features which are more intense in the spectrum of $2NH_3 \cdot H_2O$ (10% D) are designated by the letter 'b' in Table 3.5.

Features in the regions of the spectra of the partially deuterated samples that have been omitted from Figures 3.6 to 3.8 are identical with the spectral features of neat ammonia hemihydrate (Figure 3.5).

Figure 3.9 shows the spectrum of $2ND_3 \cdot D_2O$ from 4000 to 2000 cm^{-1} in the upper plot and from 2000 to 400 cm^{-1} in the lower plot. The spectrum of $2ND_3 \cdot D_2O$ (5% H) has been included, offset for clarity, in the figure in the two regions where differences in the spectral features occur due to the presence of H. The lower curve in each plot also shows the presence of a small amount of H since $2ND_3 \cdot D_2O$ actually contains 99.12 atom % D (Section 2.4). Features which grow in intensity with increased H concentration are designated with the letter 'b' in Table 3.7. An expansion of the 3450 to 2850 cm^{-1} region of the spectra of $2ND_3 \cdot D_2O$ and $2ND_3 \cdot D_2O$ (5% H) is presented in Figure 3.10. Most features are present in both spectra with a variation of intensity except that the 3140 cm^{-1} peak in the spectrum of the 1% H compound is at 3125 cm^{-1} in the spectrum of $2ND_3 \cdot D_2O$ (5% H).

Figure 3.11 shows the absorption by the intramolecular stretching vibrations in $2NH_3 \cdot H_2O$ (upper plot) and $2ND_3 \cdot D_2O$ (lower plot). The frequency scale of the lower plot is less compressed than that of the upper plot. The

features are very similar but the absorption by $2ND_3 \cdot D_2O$ is much sharper than that by $2NH_3 \cdot H_2O$. In the spectrum of the deuterated sample, the 2530/2502 cm^{-1} doublet is clearly resolved and additional features including the peak at 2326 cm^{-1} and the two weak shoulders at approximately 2265 and 2250 cm^{-1} are shown.

The spectrum of $2\ ^{15}NH_3 \cdot H_2O$ showed quite strong absorption by $^{15}NH_3 \cdot H_2O$ impurity which tended to mask some of the hemihydrate features. The impurity peaks were easily identified and frequencies of features due to $2\ ^{15}NH_3 \cdot H_2O$ which could be definitively measured are listed in Table 3.4.

CHAPTER IV.

DISCUSSION OF THE MID-INFRARED SPECTRUM

OF AMMONIA MONOHYDRATE

4.1 General

Intramolecular vibration frequencies of a molecule in a crystal differ from those of a molecule in the gas phase because of static and dynamic crystal forces (34). Static forces exerted on a molecule by the surrounding molecules cause the frequency of an uncoupled vibration to differ from the frequency of the same vibration in the gas phase. In a crystal, the equilibrium position of each molecule lies on a site of a particular symmetry. This site symmetry may be lower than the symmetry of the molecule in the gas phase. Thus, a degenerate vibration of a gaseous molecule may be split into nondegenerate uncoupled vibrations by the lower site symmetry. Site splitting may also occur if two molecules of the same chemical species occupy non-equivalent sites in the crystal. Dynamic intermolecular forces cause the uncoupled vibrations of different molecules in a crystal to couple, yielding vibrations having the symmetries of the unit cell group which is isomorphous to the point group of the crystal class. This is called Davydov splitting and when combined with site splitting, the total effect is called factor-group or unit-cell-group splitting. Those vibrations under the unit cell group which are infrared active are determined by selection rules (35-37).

Throughout this thesis, the vibrational modes of the ammonia hydrates are described by the conventional labels for the fundamental vibrations of gaseous ammonia under C_{3v} symmetry and water under C_{2v} symmetry (38).

4.2 Discussion

Interpretation of the spectrum of ammonia monohydrate may be based on the spectra of solid ammonia (39-43) and ice (44,45). A unit-cell-group analysis of the component ammonia and water molecules has been done by the correlation method (37) and the results are listed in Table 4.1.

Ammonia monohydrate crystallizes in the space group $P2_12_12_1$ (D_2^4) with four formula units occupying one set of general positions in the primitive unit cell (3). Each ammonia and water molecule lies on a site of symmetry C_1. Table 4.1 shows the relation of the molecular vibrations under the point groups, C_{3v} for ammonia and C_{2v} for water, to vibrations under the site group, C_1.

The symmetric stretching and deformation vibrations of ammonia, ν_1 and ν_2, each yield one nondegenerate site group vibration of A symmetry. The antisymmetric stretching and deformation vibrations of ammonia, ν_3 and ν_4, are degenerate under C_{3v} symmetry but the degeneracy is split under the site group yielding two nondegenerate vibrations, ν_3 and ν_3' or ν_4 and ν_4', for each degenerate mode. Rotation about the molecular z axis, R_z, yields one site group

TABLE 4.1

Correlation Table for Ammonia Monohydrate

	Molecular Group		Site Group [a]
NH_3	C_{3v}		C_1
ν_1	A_1		A
ν_2	A_1		A
ν_3	E	ν_3	A
		ν_3'	A
ν_4	E	ν_4	A
		ν_4'	A
R_z	A_2		A
R_x, R_y	E		A
			A
H_2O	C_{2v}		C_1
ν_1	A_1		A
ν_2	A_1		A
ν_3	B_1		A
R_z	A_2		A
R_x	B_2		A
R_y	B_1		A

[a]Under the Unit Cell Group D_2, A of the site group yields $A+B_1+B_2+B_3$. All modes are Raman active and B_1, B_2 and B_3 are infrared active.

vibration of A symmetry, while R_x and R_y, which are degenerate under C_{3v}, yield two vibrations of A symmetry under C_1.

Each vibration and rotation of the water molecule is nondegenerate under C_{2v} and, therefore, yields one site group vibration of A symmetry.

Each nondegenerate site group vibration is split by intermolecular coupling under the unit cell group, D_2, to yield four vibrational components of symmetry $A + B_1 + B_2 + B_3$. All modes are Raman active and B_1, B_2 and B_3 modes are infrared active.

Assignment of the N-H stretching and HNH deformation frequencies of ammonia monohydrate (Table 3.3) may be made by analogy with solid ammonia. Solid ammonia has C_3 site symmetry and forms N-H$\cdots$N hydrogen bonds of length 3.342 $\overset{o}{A}$ at 77°K (32,46,47). Ammonia monohydrate, the structure of which has been discussed in Section 1.3, contains N-H$\cdots$O hydrogen bonds of length 3.21, 3.26 and 3.29 $\overset{o}{A}$, which are roughly equivalent (1,48) to N-H$\cdots$N bonds of length 3.31 to 3.39 $\overset{o}{A}$. The N-H$\cdots$O bonds are very weak hydrogen bonds since they are 0.3 $\overset{o}{A}$ longer than the sum of the van der Waal radii of oxygen and nitrogen (49) which is 2.9 $\overset{o}{A}$. Since these hydrogen bonds are weak, it is expected that the N-H stretching frequency of each bond will be similar and thus, the stretching vibrations will approximate those of a molecule having C_3 symmetry, such as in solid ammonia.

In infrared spectra of solid ammonia at 60 to 100°K (39-43), the doubly degenerate antisymmetric stretching vibration, ν_3, is reported at ~3370 cm^{-1} while the symmetric stretching vibration, ν_1, and overtone, $2\nu_4$, of the antisymmetric deformation are reported in Fermi resonance at 3205/3290 cm^{-1}. The intensity of the overtone is enhanced by Fermi resonance with ν_1. The unperturbed ν_1 vibration is predicted to occur at ~3250 cm^{-1} (41). The intensity of ν_3 is very strong relative to $\nu_1/2\nu_4$. Therefore, the very intense doublet at 3402/3387 cm^{-1} in the monohydrate spectrum (Figures 3.1 and 3.2) is assigned to ν_3 and ν_3'. Further evidence for this assignment was obtained from the frequency shifts under ^{15}N substitution (Table 3.3).

Assuming an ammonia molecule of C_{3v} symmetry, isotopic frequency shifts were calculated under the harmonic approximation (50). Shifts of about 3 cm^{-1} for stretching vibrations of A_1 symmetry and 9 cm^{-1} for those of E symmetry were calculated. The observed shifts of 6 to 8 cm^{-1} confirm the assignment of the doublet to the antisymmetric N-H stretching vibrations. The infrared spectrum of ^{15}NH$_3 \cdot$H$_2$O shows three distinct features in this region. The 3384 cm^{-1} feature corresponds to a weak uncertain shoulder at 3392 cm^{-1} in the spectrum of ^{14}NH$_3 \cdot$H$_2$O (Figure 3.2). Assuming the assignment of the doublet is correct, this third feature may arise from unit-cell-group splitting. The assignment of the doublet has been based

on the assumption that site splitting is much greater than unit-cell-group splitting. This is reasonable since six features, $2B_1 + 2B_2 + 2B_3$, are expected from unit-cell-group splitting.

The weak features at 3330, 3305, 3287 and 3270 cm^{-1} are assigned to $\nu_1/2\nu_4$. It is expected that three of the frequencies are due to $2\nu_4$ which has three components of A symmetry under the site group (51).

Although the doubly degenerate antisymmetric deformation of ammonia, ν_4, yields two components under the site group, three features at 1664, 1650 and 1625 cm^{-1} are assigned to ν_4 (Figure 3.3). The same situation arises for the symmetric deformation, ν_2. Two features at 1133 and 1095 cm^{-1} are assigned to ν_2 (Figure 3.4) but only one component is expected under the site group. The frequencies observed for these features in $^{15}NH_3 \cdot H_2O$ (Table 3.3) agree well with the shifts expected, about 2 cm^{-1} for ν_4 and 5 cm^{-1} for ν_2, under these assignments. The extra peaks for ν_2 and ν_4 may arise from coupling. However, inter-molecular coupling is not expected to occur extensively in ammonia monohydrate since each ammonia molecule is surrounded by water molecules having very different vibrational frequencies. It has also been reported (41) that intermolecular coupling between ammonia molecules is weak in solid ammonia although each ammonia molecule is surrounded by four ammonia molecules with equivalent N-H bonds. The appearance of the extra features for ν_2 and ν_4

cannot, therefore, be readily explained by the presently available information.

Assignment of the O-H stretching and HOH deformation features (Table 3.3) was made by analogy with ice (44,45) and with the aid of recent correlations (26,48,52-54) of bond lengths with frequency. Several empirical relations have been proposed for hydrogen bonded systems, A-H···B, correlating the A-H stretching frequency, ν(A-H), with the A···B distance, R(A···B). These relations show considerable scatter of data points indicating the influence of factors on the A-H stretching frequency other than the A···B bond length. Although such correlations are only approximate, they generally show the trend of increasing ν(A-H) with increasing R(A···B). Ammonia monohydrate contains O-H···O bonds of length 2.76 Å and O-H···N bonds of length 2.775 Å. Since general correlations of ν(O-H) with O-H···N bond lengths are not available, correlations relating ν(O-H) with O-H···O bond lengths have been used assuming the 2.775 Å O-H···N bond to be equivalent (1,48) to an O-H···O bond of length 2.675 Å. The correlations predict O-H stretching frequencies near 3250 and 3000 cm^{-1} for O···O distances of 2.76 and 2.675 Å, respectively, with a possible error of about ±100 cm^{-1} in these predictions. Thus, the 3190 cm^{-1} band (Figures 3.1 and 3.2) is assigned to the O-H stretching vibration of the 2.76 Å O-H···O bond and the 2910 cm^{-1} band is assigned to the O-H stretching vibration of the 2.775 Å O-H···N bond. The weak feature at

1540 cm^{-1} (Figure 3.3) is assigned to the deformation, ν_2, of water.

The lower frequency peaks, 908 to 448 cm^{-1} (Table 3.3, Figure 3.4), are assigned to rotational modes of water and ammonia. No additional information concerning the assignment of the rotational modes is gained from the spectrum of $^{15}\text{NH}_3 \cdot \text{H}_2\text{O}$. Moment of inertia calculations (55) for ammonia having C_{3v} symmetry predict a frequency shift, under ^{15}N substitution, of 0.8 to 0.4 cm^{-1} in the 900 to 400 cm^{-1} region. Such a shift is too small to detect in the spectra obtained.

Intermolecular coupling has been neglected in making these assignments. In the spectra of different phases of ice (44,56-58), the O-H stretching frequencies are spread over a broad range because of the combined effects of inter- and intra-molecular coupling. This range is about equal to the 280 cm^{-1} difference between $\nu_{OH\cdots O}$ and $\nu_{OH\cdots N}$ of ammonia monohydrate. It is, therefore, believed that intermolecular coupling has little effect on the O-H stretching frequencies of ammonia monohydrate. This is understandable since each water molecule in ammonia monohydrate has only two nearest-neighbour water molecules with which to couple. The water molecules in the ices, on the other hand, have four nearest-neighbours with similar uncoupled vibration frequencies.

In ammonia monohydrate, X-ray diffraction studies (3) have not located the hydrogen atom positions for the hydrogens in the O-H···O bonds forming the chains of water molecules. Although the hydrogens must be ordered within each chain, there is a possibility of disorder from chain to chain. The two possible arrangements of the hydrogen atoms form N···H-O-H···O angles of $110.7 \pm 0.2°$ and $111.4 \pm 0.2°$ (3). The small difference between these angles does not provide a basis for choosing a preferred hydrogen arrangement. The mid-infrared spectrum of ammonia monohydrate gives no clear indication of structural order or disorder. Some of the bands are broad indicating possible disorder, but the infrared spectra of fully ordered phases of ice (57,59) also show broad bands. The sharp features assigned to ν_R, on the other hand, indicate that the structure of the monohydrate may be ordered (57,59,60).

It has been shown that far-infrared absorption by translational lattice vibrations can distinguish between ordered and orientationally disordered forms of ice (60,61). The far-infrared spectra of the ordered phases of ice show sharp discrete absorption lines, while the far-infrared of disordered forms of ice show continuous broad absorption due to the activation of all of the vibrations by the disorder. Therefore, the far-infrared spectrum of ammonia monohydrate should give an indication of order or disorder in the structure.

Furthermore, mid-infrared studies of partly deuterated ammonia monohydrate would give the frequencies of isolated N-H and O-H stretching vibrations, which would provide more information concerning the degree of intermolecular coupling (62,63).

CHAPTER V.

DISCUSSION OF THE MID-INFRARED SPECTRA

OF AMMONIA HEMIHYDRATE

5.1 General

The initial assignment of the mid-infrared spectrum of ammonia hemihydrate will be based on the spectra of solid ammonia (39-43) and ice (44,45) as well as group theoretical considerations.

The structure of ammonia hemihydrate is described in Section 1.3 of this thesis. To review, it is known that ammonia hemihydrate crystallizes in the standard (4,19) centrosymmetric space group Pnma (D_{2h}^{16}). There are four formula units per unit cell and each ammonia and water molecule occupies a site of C_S symmetry, that is, each heavy atom sits on a mirror plane. The ammonia hemihydrate structure at 178°K contains two non-equivalent types of ammonia molecules distinguished by their hydrogen bonding. Molecules of type I (4) receive one O-H···N bond of length 2.83 Å (2.82 Å at 100°K) and form three N-H···O bonds of length 3.11, 3.24 and 3.24 Å. Molecules of type II receive one O-H···N bond of length 2.85 Å (2.84 Å at 100°K) and the remaining hydrogens of the ammonia molecule are unbound. It is believed that this ammonia molecule re-orients about its single hydrogen bond above 52°K (4,6), thus, possibly disturbing the Pnma symmetry of the crystal.

As in the case of the monohydrate, the vibrations of ammonia hemihydrate will be described by the conventional labels for the vibrations of ammonia gas and water vapor (38). A unit-cell-group analysis (37) of the component ammonia and water molecules yielded the results listed in Table 5.1. The table correlates the molecular vibrations under the symmetries of the gas phase, the site group and the unit cell group. Only one ammonia molecule is considered since the results apply to both types.

The correlation table shows that each of the symmetric stretching and deformation vibrations, ν_1 and ν_2, of ammonia yields one vibration of A' symmetry under the site group, C_s. The degenerate antisymmetric stretching and deformation vibrations, ν_3 and ν_4, are each split under the site group to yield two nondegenerate vibrations of A' and A" symmetry. These vibrations are denoted by ν_3' and ν_3'' or ν_4' and ν_4'' in the table. Rotation about the molecular z axis yields, under the site group, one nondegenerate vibration which is antisymmetric with respect to the mirror plane. Rotations about the x and y axes, which are degenerate under C_{3v}, split to yield two nondegenerate vibrations of A' and A" symmetry under C_s.

For water, the symmetric stretching and deformation vibrations, ν_1 and ν_2, as well as the antisymmetric stretching vibration, ν_3, are all nondegenerate under C_{2v} and, therefore, each yields one vibration of A' symmetry under the site group, the symmetry plane of which is the

TABLE 5.1

Correlation Table for Ammonia Hemihydrate

NH₃	Molecular Group C_{3v}		Site Group[a] C_s (ac)
ν_1	A_1		A'
ν_2	A_1		A'
ν_3	E	ν_3'	A'
		ν_3''	A''
ν_4	E	ν_4'	A'
		ν_4''	A''
R_z	A_2		A''
R_x, R_y	E		A'
			A''

H_2O	C_{2v}	C_s (ac)
ν_1	A_1	A'
ν_2	A_1	A'
ν_3	B_1	A'
R_z	A_2	A''
R_x	B_2	A''
R_y	B_1	A'

[a]Under the Unit Cell Group, D_{2h}, A' of the site group yields $A_g + B_{1u} + B_{2g} + B_{3u}$ and A'' of the site group yields $A_u + B_{1g} + B_{2u} + B_{3g}$, if the correspondence between the axes of the crystal and the point group is chosen to be $a \equiv x$, $b \equiv y$, $c \equiv z$. B_{1u}, B_{2u} and B_{3u} are infrared active, A_g, B_{1g}, B_{2g} and B_{3g} are Raman active and A_u is inactive in both the infrared and the Raman.

molecular plane. Rotations about the x and z axes of the molecule yield one site group vibration of A" symmetry each while rotation about the y axis yields a vibration of A' symmetry.

These site group vibrations undergo further splitting by means of intermolecular coupling under the unit cell group, D_{2h}. By choosing the point group axes, x, y and z, and the crystal axes, a, b and c, so that a≡x, b≡y and c≡z, the site group vibration A' yields the vibrational components $A_g + B_{1u} + B_{2g} + B_{3u}$ while A" yields $A_u + B_{1g} + B_{2u} + B_{3g}$ under D_{2h}. B_{1u}, B_{2u} and B_{3u} are infrared active, all the gerade modes are Raman active and A_u is inactive in both the infrared and the Raman.

5.2 The Infrared Spectrum of $2NH_3 \cdot H_2O$

In the infrared spectrum of ammonia hemihydrate, the high-frequency doublet (Figures 3.2 and 3.5) is assigned (Table 3.4) to the antisymmetric N-H stretching vibration, ν_3, by analogy with the spectrum of solid ammonia (39-43). The observed 23 cm^{-1} separation of the two peaks may be due to site splitting, multiple-site splitting or to unit-cell-group splitting. The site splitting occurs because under the site group, C_s, the degeneracy of the antisymmetric N-H stretching vibration of each ammonia molecule is lost yielding A' and A" components which may be responsible for the doublet if the absorptions by the

two types of ammonia molecules coincide. Multiple-site splitting is due to the two types of ammonia molecules and could cause the doublet if the site splitting, due to the loss of degeneracy, is too small to resolve. If unit-cell-group splitting is considered, one would expect a total of 6 infrared-active components, $2B_{1u} + 2B_{2u} + 2B_{3u}$, from the two types of ammonia molecules.

It should be noted that the high-frequency doublet in the spectrum of ammonia hemihydrate is much broader than the corresponding doublet in the spectrum of ammonia monohydrate (Figure 3.2). As stated in Chapter IV, ammonia monohydrate also has 6 infrared-active components, $2B_1 + 2B_2 + 2B_3$, under the unit cell group, D_2, for the antisymmetric N-H stretching vibration, ν_3. Therefore, the broadness of the doublet observed in the spectrum of the hemihydrate is probably not simply due to the merging of the unit-cell-group components.

One explanation for the broadness of the doublet may be the disorder in the orientations of the $N_{II}H_3$ molecules. As mentioned previously, the $N_{II}H_3$ molecules are believed to reorient above 52°K, thus causing disorder of the hydrogen atom positions. This disorder may destroy the selection rules, thus causing the infrared activity of all the crystal vibrations based on the A' and A" components of ν_3 of each type of ammonia. There are 6×10^{23} such crystal vibrations from each component of each molecule

per mole of $2NH_3 \cdot H_2O$, each of which has a slightly different frequency due to intermolecular vibrational coupling. Thus, the increased number of infrared-active vibrations would cause the broadness of the doublet. The origin of the two peaks of the doublet could, in this situation, be either of the site splittings discussed above.

The symmetric stretching vibration of ammonia, ν_1, and the overtone of the antisymmetric deformation vibration, $2\nu_4$, are not observed in the spectrum. These features are probably masked by the broad absorption from 3350 to 3200 cm^{-1} (Figure 3.2). This is not surprising as the absorption by these vibrations is weak in solid ammonia.

The remaining general assignments of the ammonia vibrations, ν_4 near 1600 cm^{-1}, ν_2 near 1100 cm^{-1} and ν_R near 500 cm^{-1}, were based on the infrared spectrum of solid ammonia. These spectral features are presented in Figure 3.5 and the corresponding frequencies are listed in Table 3.4.

It should be noted that the 70 cm^{-1} separation between the extreme features of $\nu_2(NH_3)$ is rather large relative to the 23 cm^{-1} split observed for $\nu_3(NH_3)$. It is possible that the 1156 cm^{-1} feature is an overtone or combination band which borrows intensity from the fundamental ν_2 vibration through Fermi resonance (64). There

is also a rather large 70 cm^{-1} separation between the extreme features assigned to $\nu_4(NH_3)$. However, the fundamental vibration $\nu_2(H_2O)$ also absorbs in this region, thus complicating the assignment.

The O-H stretching vibrations have been assigned (Table 3.4) on the basis of correlations (26,48,52-54) between the O-H stretching frequency, $\nu(O-H)$ and the $O\cdots O$ distance, $R(O-H\cdots O)$ described in Chapter IV. In ammonia hemihydrate, the O-H stretching vibrations are those in the $O-H\cdots N_I$ and $O-H\cdots N_{II}$ bonds of length 2.82 Å and 2.84 Å, respectively, at 100°K. Since the only correlations available relating $\nu(O-H)$ with $O-H\cdots N$ bond lengths (2) are for particular systems and are not generally applicable, the above mentioned $O\cdots O$ distance correlations have been used. To use these correlations, the $O-H\cdots N$ bond length was adjusted by 0.1 Å, the difference between the van der Waals radii of oxygen and nitrogen (49), to yield the equivalent (1,48) $O-H\cdots O$ bond lengths, 2.72 and 2.74 Å. These correlations are rough approximations but lead to the assignment of the 3125 cm^{-1} peak to the 2.84 Å $O-H\cdots N_{II}$ bond and the 2975 cm^{-1} peak to the 2.82 Å $O-H\cdots N_I$ bond.

The observed separation of the two peaks is considerably greater than the ~40 cm^{-1} separation predicted for $O-H\cdots O$ bonds which differ in length by only 0.02 Å. However, the assignment, which attributes the two peaks

to site splitting, is believed to be correct for three
reasons. First, the predictions are approximate. Second,
a graph of the absorption frequencies of O-H bonds of H_2O,
which form O-H$\cdots$N bonds in hexamethylenetetramine hexa-
hydrate (1), ammonia monohydrate and ammonia hemihydrate,
versus the O-H$\cdots$N bond lengths (Figure 5.1) shows that
all of the points would be on a smooth curve if the 2.82 Å
O-H$\cdots$N bond was really 2.80 Å long. This is quite pos-
sible since the error limits of the X-ray determination
of the bond lengths was ±0.02 Å for each bond. Third,
the only other possible origin of the two peaks is inter-
molecular vibrational coupling which is expected to be too
small to cause vibrational frequencies to separate by 150
cm^{-1} because each water molecule is surrounded by ammonia
molecules which have very different vibrational frequen-
cies.

The assignments of features to $\nu_2(H_2O)$ and $\nu_R(H_2O)$
(Table 3.4) are made by analogy with ice (44). The $\nu_2(H_2O)$
vibration absorbs in the same region as $\nu_4(NH_3)$, so a
more definitive assignment cannot be made from the avail-
able information.

5.3 Studies of Isotopically Substituted Ammonia Hemihydrate

To gain further evidence on the assignment of the
spectrum of ammonia hemihydrate, several isotopically sub-
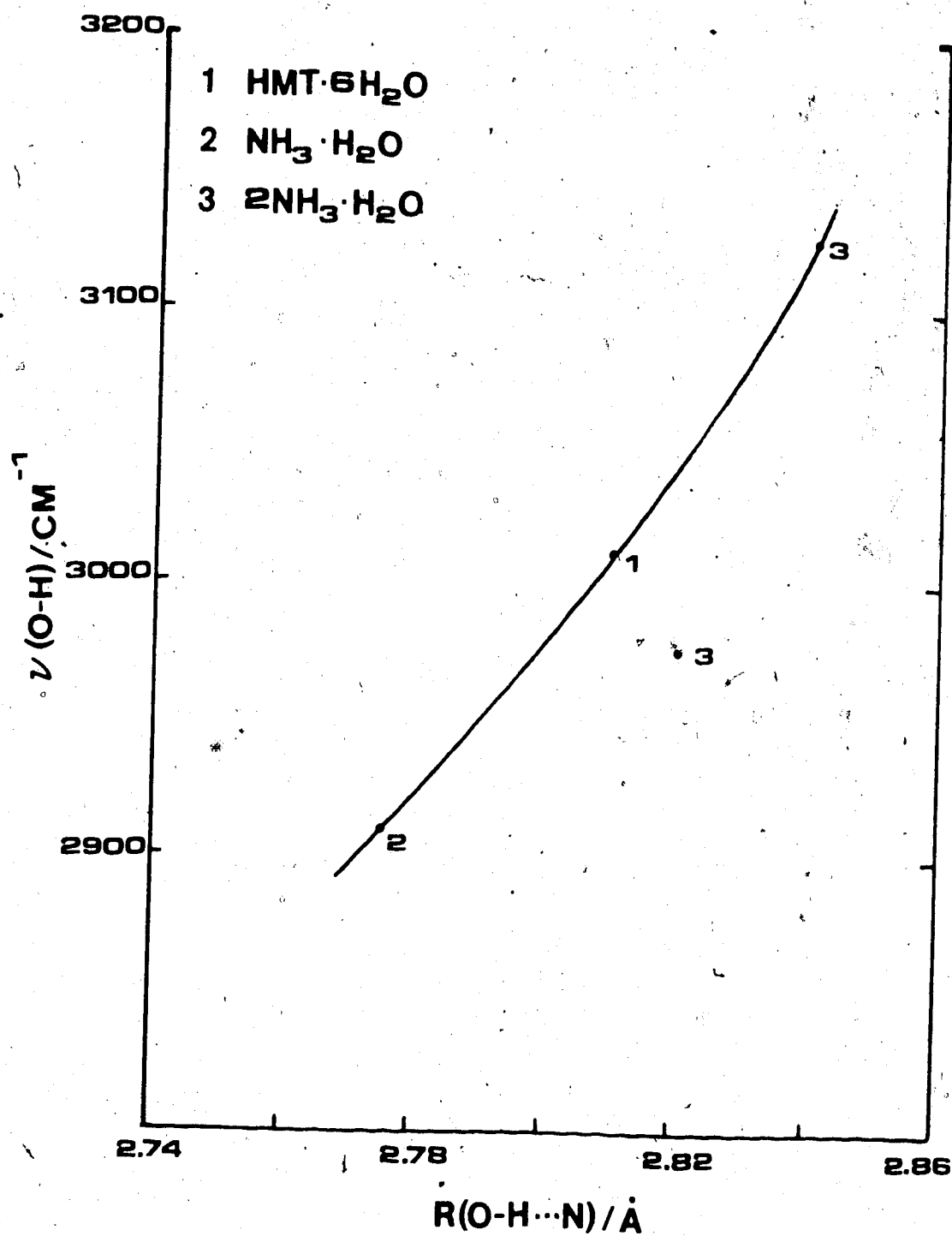
Figure 5.1 Graph of ν(OH) versus R(O-H···N) for
1) Hexamethylenetetramine Hexahydrate abbreviated
HMT·6H₂O 2) Ammonia Monohydrate and 3) Ammonia.
Hemihydrate.

stituted samples were studied. These shall now be dis-
cussed in detail.

5.3.1 The Infrared Spectrum of 2 $^{15}NH_3 \cdot H_2O$

The frequencies which could be definitively measured
from the spectrum of 2 $^{15}NH_3 \cdot H_2O$ are listed in Table 3.4.
The expected frequency shifts under ^{15}N substitution were
calculated under the harmonic approximation (50) for
ammonia molecules of C_{3v} symmetry. The N-H stretching
frequencies are so different from the NH_3 deformation
frequencies that the interaction between the two can be
ignored to an excellent approximation (65). Under these
conditions the vibration frequencies of ammonia are given
by the expressions in Table 5.2, where the F's are force
constants and the G's are properties of the molecular
geometry which are tabulated (50,66). The $\hat{G}$ values
were calculated for $^{14}NH_3$ and $^{15}NH_3$ from the atomic mas-
ses (23) and the values 106.8° and 1.01 Å for the HNH
angle and N-H distance (32). The force constants are in-
variant to isotopic substitution under the harmonic ap-
proximation, so the ratio of the frequencies of isotopic
molecules is the square root of the ratio of the corres-
ponding terms in G. This is an approximation for the
ammonia molecules of C_s symmetry in the hemihydrate.

The frequency shift calculated for the symmetric N-H
stretching vibration, ν_1, is about 3 cm^{-1} and that calcu-

TABLE 5.2

Expressions for the Vibrational Frequencies of an

Ammonia Molecule of C_{3v} Symmetry

<u>Intramolecular Vibrations:</u>

$$\nu_1 = (2\pi c)^{-1} \left\{ [G_{rr}^2 + 2G_{rr}^1] [F_{rr} + 2F_{rr}'] \right\}^{\frac{1}{2}}$$

$$\nu_2 = (2\pi c)^{-1} \left\{ [G_{\phi\phi}^3 + 2G_{\phi\phi}^2 \left(\tfrac{1}{1}\right)] [F_{\phi\phi} + 2F_{\phi\phi}'] \right\}^{\frac{1}{2}}$$

$$\nu_3 = (2\pi c)^{-1} \left\{ [G_{rr}^2 - G_{rr}^1] [F_{rr} - F_{rr}'] \right\}^{\frac{1}{2}}$$

$$\nu_4 = (2\pi c)^{-1} \left\{ [G_{\phi\phi}^3 - G_{\phi\phi}^2 \left(\tfrac{1}{1}\right)] [F_{\phi\phi} - F_{\phi\phi}'] \right\}^{\frac{1}{2}}$$

G_{rr}^2, G_{rr}^1, $G_{\phi\phi}^3$ and $G_{\phi\phi}^2 \left(\tfrac{1}{1}\right)$ are defined in reference 66. They are properties of the molecular geometry and atomic masses.

The potential energy of vibration is given by:

$$V = \tfrac{1}{2} \left[\sum_{i=1}^{3} (F_{rr} R_i^2 + F_{\phi\phi} \phi_i^2) + \sum_{i=1}^{3} \sum_{j=1}^{3} (F_{rr}' R_i R_j + F_{\phi\phi}' \phi_i \phi_j) \right]$$

where the R_i are the bond stretching displacements and the ϕ_i are the HNH angle displacements.

<u>Rotational Vibrations:</u>

$$\nu_i = (2\pi c)^{-1} (F/I_i)^{\frac{1}{2}}$$

where F is the force constant and I_i is one of the three moments of inertia.

lated for the antisymmetric stretch, ν_3, is about 9 cm^{-1}. The observed shift of 8 cm^{-1} for the 3374 cm^{-1} feature of the doublet confirms its assignment to the antisymmetric N-H stretching vibration. Unfortunately, the 3397 cm^{-1} peak of the doublet was masked by ^{15}NH$_3$·H$_2$O impurity. The calculated shift for the symmetric deformation, ν_2, of an ammonia molecule is about 5 cm^{-1} and the shift for the antisymmetric deformation, ν_4, is about 2 cm^{-1}. The observed shifts of the features at 1156/1092/1083 cm^{-1} are 2, 4 and 7 cm^{-1}, respectively, under ^{15}N substitution. The two lower-frequency features are thus correctly assigned to the symmetric deformation of ammonia. The 2 cm^{-1} shift of the 1156 cm^{-1} peak may indicate that this feature is not due to ν_2(NH$_3$). However, this shift is a rough estimate as mulling agent absorption obscures the peak maximum. The frequency shifts observed near 1600 cm^{-1} are 1 to 3 cm^{-1} confirming their assignment to ν_4.

The ratio of the frequencies of corresponding rotational vibrations of two isotopic forms of ammonia is, to first approximation, the inverse ratio of the square roots of the corresponding moments of inertia (Table 5.2). Calculations of the moments of inertia based on the structural data given earlier showed that rotational vibrations between 400 and 900 cm^{-1} shift by less than 1 cm^{-1} on ^{15}N substitution. Such a shift is too small to detect for bands as broad as those observed (Figure 3.4) so the ro-

tational vibrations of ammonia could unfortunately not be identified by ^{15}N substitution.

5.3.2 The Infrared Spectrum of $2ND_3 \cdot D_2O$

The infrared spectra of $2ND_3 \cdot D_2O$ are shown in Figures 3.9 - 3.11 and the frequencies and assignments are listed in Table 3.7.

Corresponding features in the spectra of $2ND_3 \cdot D_2O$ and $2NH_3 \cdot H_2O$ (Figures 3.5, 3.11) are readily identified by the analogous band shapes. The frequencies of equivalent features in the spectra are listed in Table 5.3 along with the observed isotopic shifts, ν_H/ν_D. The obvious relation of the band shapes and frequencies of most of the features indicates that these features are due to fundamental transitions and that the enhancement of the intensities of overtone or combination bands by Fermi resonance does not greatly affect the major bands.

One notable difference between the spectra of $2ND_3 \cdot D_2O$ and $2NH_3 \cdot H_2O$ is the shape of the band due to the overlapping absorptions by $\nu_4(NH_3)$ and $\nu_2(H_2O)$. It has been shown in the Raman (67) and infrared (68) spectra of ice 1h that the band due to $\nu_2(H_2O)$ sharpens considerably on deuteration and a similar effect undoubtedly explains the change observed in the hemihydrate spectra.

Another difference between the spectra is the strong, sharp feature at 2326 cm^{-1} in $2ND_3 \cdot D_2O$ which has no

TABLE 5.3

Equivalent Features in the Spectra of $2NH_3 \cdot H_2O$,
$2ND_3 \cdot D_2O$, $2NH_3 \cdot H_2O$ (5 or 10%D) and $2ND_3 \cdot D_2O$ (5%H) [a]

$2NH_3 \cdot H_2O$ ν/cm^{-1}	$2ND_3 \cdot D_2O$ ν/cm^{-1}	ν_H/ν_D	$2ND_3 \cdot D_2O$ (5%H) ν/cm^{-1}	$2NH_3 \cdot H_2O$ (5 or 10%D) ν/cm^{-1}	ν_H/ν_D
3397(2)	2530(2)	1.343(2)	3355(5)	~2481	1.35
3374(2)	2502(2)	1.348(2)	3322(2)	2445(2)	1.359(2)
3125(10)	2355(5)	1.327(7)	3308(2)	2432(2)	1.360(2)
2975(10)	2230(2)	1.334(6)	3125(5)	2347(4)	1.331(4)
2500(4)	~1840	1.36	~3050 sh	2275(15)	1.340
2294(2)	1705(5)	1.345(5)	962(2)	964(2)	1.0
1626(2)	~1210	1.34	936(2)	936(2)	1.0
1590(2)	1182(2)	1.345(4)			
1555(1)	~1160	1.34			
1156(2)	884(3)	1.308(7)			
1092(2)	848(2)	1.288(5)			
1083(2)	838(2)	1.292(6)			
~882	646(2)	1.36(1)			
817(2)	606(2)	1.35(1)			
767(2)	560(2)	1.37(1)			

[a] The estimated uncertainties in the last figure are given in brackets.

counterpart in $2NH_3 \cdot H_2O$. This feature could be due to the symmetric stretching vibration of ammonia, ν_1, calculated to be at ~2350 cm^{-1} (Section 5.3.3). However, the intensity of this feature makes this assignment unlikely since ν_1 absorbs very weakly in $2NH_3 \cdot H_2O$ and solid ammonia (39-43).

Another plausible explanation for this feature can be made if attention is shifted to the sharp minimum at 2333 cm^{-1}. The appearance of such a sharp dip in a broad band is characteristic of an Evans hole (69,70) When a transition that yields sharp, weak absorption is in Fermi resonance with transitions that yield broad, strong absorption, the perturbation causes a loss of absorption intensity in the narrow region of the weak transition and a gain in other regions. This yields, within a broad band, a narrow region of increased transmission known as an Evans hole. Thus, the observed dip at 2333 cm^{-1} in the spectrum of $2ND_3 \cdot D_2O$ could be an Evans hole arising from Fermi resonance between the overtone, $2\nu_2 (D_2O)$ or $2\nu_4 (ND_3)$, the fundamental absorption of which occurs at ~1170 cm^{-1}, and the broad $\nu_{OD}(D_2O)$ band.

As in the case of ice (44,68), the absorption by the stretching vibrations of N-H and O-H bonds is broader than that by N-D and O-D bonds (Figure 3.11). This indicates that the former are more affected by anharmonicity and that the N-D and O-D stretching bands are more likely

to be explainable by harmonic oscillator models.

Comparison of the splittings observed in the spectra of $2NH_3 \cdot H_2O$ and $2ND_3 \cdot D_2O$ provides information concerning the source of the splittings. In general, when a splitting is caused by the vibrational potential energy, the splittings of deuterated species are smaller than those of the hydrogenated species by the same ratio as the frequency shifts. This is the case for most of the bands in the spectra of the hemihydrate, but there are two interesting cases.

The separation of the doublet assigned to $\nu_3(NH_3)$ is 23 cm^{-1}, while the doublet assigned to $\nu_3(ND_3)$ has a separation of 28 cm^{-1}. The immediate interpretation of such a situation is that the splitting arises from kinetic coupling, (that is, the interaction of displacements of adjacent bonds through a common atom. This effect explains the observed greater difference between the symmetric and antisymmetric stretching frequencies in gaseous ND_3 or D_2O than in gaseous NH_3 or H_2O. This effect of kinetic coupling can also be detected in the spectra of the ices and solid ammonia (41). Thus, the greater splitting of the doublet in $2ND_3 \cdot D_2O$ than in $2NH_3 \cdot H_2O$ suggests that kinetic coupling causes the splitting, which implies that the splitting has an intramolecular origin. In terms of the explanations suggested in Section 5.2, this observation appears to support the inter-

pretation that the splitting is due to the A' and A" site group components of $\nu_3(NH_3)$, with the absorption by the two types of molecules coincident. As will be seen in Section 5.3.3, however, this interpretation is not supported by calculations, and the splitting, and its increase on deuteration, appears to arise from the two types of ammonia molecules. This result is surprising and emphasizes the need for care in interpreting the spectra of crystals in which two sites are occupied by the same chemical species.

Another unusual splitting is in the band due to $\nu_2(NH_3)$ which is at 1156/1092/1083 cm^{-1} in the spectrum of $2NH_3 \cdot H_2O$ (Figure 3.5) and 884/848/838 cm^{-1} in the spectrum of $2ND_3 \cdot D_2O$ (Figure 3.9). For $2NH_3 \cdot H_2O$, the observed splitting of the two high-frequency features is 64 cm^{-1} compared to a splitting of 36 cm^{-1} for $2ND_3 \cdot D_2O$. The ratio 64/36 is much larger than the ratio of the frequencies, ~1.3, indicating that the high-frequency features at 1156 and 884 cm^{-1} may not be components of ν_2. This was suggested earlier by the unusually large split between the extreme features of ν_2 relative to the small split of ν_3 in the spectrum of $2NH_3 \cdot H_2O$ and by the small ^{15}N isotopic shift of the 1156 cm^{-1} feature.

The splitting of the two low-frequency features of ν_2 is about 10 cm^{-1} in the spectra of both $2NH_3 \cdot H_2O$ and $2ND_3 \cdot D_2O$. This splitting must be due either to inter-

molecular effects arising from unit-cell-group splitting into the infrared-active components, $B_{1u} + B_{3u}$, or to the existence of the two types of ammonia molecules.

5.3.3 Infrared Spectra of Isotopically Dilute Samples

Valuable information concerning the origin of observed spectral splittings may be gained from the study of isotopically-mixed crystals. In a dilute solid solution of a deuterated compound in the undeuterated host compound, or vice versa, the static crystalline forces which determine the site symmetry are identical to those of the pure crystals (62,63). Any isotopic impurity introduced into the pure crystal occupies at random all available sites in the crystal. In dilute mixtures, the isotopic impurity is surrounded by the host species so that the intermolecular coupling is essentially eliminated unless frequencies of the impurity are close to those of the host. The vibration frequencies of the impurity are the uncoupled frequencies which show the site splitting.

To investigate the splittings observed in the spectrum of ammonia hemihydrate, the spectra of $2NH_3 \cdot H_2O$ (5% D), $2NH_3 \cdot H_2O$ (10% D) and $2ND_3 \cdot D_2O$ (5% H) were studied. The percentages of NH_2D, ND_2H, HOD, NH_3, ND_3 and H_2O expected in each of these isotopic mixtures assuming equal distribution between all sites are listed in Table 5.4. The interpretation of the absorption by the dilute isotopic

TABLE 5.4

Percentages of Isotopic Species

in Dilute Isotopically Substituted Samples

Isotopic Species	$2NH_3 \cdot H_2O$ (5%D)	$2NH_3 \cdot H_2O$ (10%D)	$2ND_3 \cdot D_2O$ (5%H)
NH_3	85.7	72.9	0.01
NH_2D	13.5	24.3	0.7
ND_2H	0.7	2.7	13.5
ND_3	0.01	0.1	85.7
H_2O	90.3	81.0	0.3
HOD	9.5	18.0	9.5
D_2O	0.3	1.0	90.3

impurities is complicated by the fact that they are not fully isotopically substituted, that is, they are, for example, NH_2D and HOD in $2NH_3 \cdot H_2O$ instead of ND_3 and D_2O in $2NH_3 \cdot H_2O$.

Thus, in order to interpret the spectra of these vibrationally-isolated species, the structure of ammonia hemihydrate must be considered. The ammonia molecule of type I has two non-equivalent types of hydrogen atoms, one lying on the mirror plane while the other two hydrogen atoms are symmetrically equivalent under the reflection operation. The spectra of dilute isotopic substituents indicate the number of different sites available. Thus, in the spectra of isotopically dilute ND_2H or NH_2D, two bands are expected for the isolated N-H or N-D stretching vibrations of each type I ammonia molecule, one being twice as intense as the other, and two bands are expected for the HND deformation vibration, again with a 2:1 intensity ratio. Because there are two types of ammonia molecules in the structure, each with C_s symmetry, four bands are expected from the N-H or N-D stretching vibrations and four from the HND deformation vibrations. In each case, two bands should be twice as intense as the other two.

If the possible disorder of the type II ammonia molecule is considered, one may expect a continuous range of sites available for the hydrogen atoms of $N_{II}H_3$ or, if

only the two orientations (related by a 60° rotation) which preserve the plane of symmetry are occupied, then one would expect four spectral bands of intensity ratio 1:2:2:1 for each, the N-D stretching vibration and the HND deformation vibration of vibrationally isolated $N_{II}H_2D$ or $N_{II}D_2H$.

The spectra of $2NH_3 \cdot H_2O$ (5% D) and $2NH_3 \cdot H_2O$ (10% D) are presented in Figures 3.6 - 3.8 and spectra of $2ND_3 \cdot D_2O$ (5% H) are presented in Figures 3.9 and 3.10. The general assignments are listed in Tables 3.5 and 3.7. The features from 2501 to 2432 cm^{-1} (Figure 3.6) are assigned to the isolated N-D stretching vibrations and the two broad features at 2347 and 2275 cm^{-1} are assigned to the stretching vibrations of the isolated O-D bonds of length 2.84 and 2.82 Å, respectively. The two peaks at 1056 and 1021 cm^{-1} (Figure 3.8) are assigned to the symmetric deformation of NH_2D and the two features at 964 and 936 cm^{-1} are assigned to the same vibration of ND_2H. The spectrum of $2NH_3 \cdot H_2O$ (10% D) clearly shows the latter two peaks. The appearance of these peaks may be understood from the percent of NH_2D and ND_2H expected, 24.3 and 2.7%, respectively, for 10% D (Table 5.4). The two low-frequency peaks at 650 and 630 cm^{-1} are assigned to the rotational displacements of HOD. The remaining assignments are analogous to those of the spectrum of $2NH_3 \cdot H_2O$.

In the spectrum of $2ND_3 \cdot D_2O$ (5% H) (Figure 3.10), the high-frequency features from 3360 to 3308 cm^{-1} are assigned to the isolated N-H stretching vibrations. The spectrum of neat $2ND_3 \cdot D_2O$ also shows these features due to the ~1% H impurity. It should be noted that the featureless band at 3355 cm^{-1} in the spectrum of 5% H corresponds to the four features at 2501/2490/2473/2461 cm^{-1} in the isolated N-D stretching region. A similar effect occurs in the spectrum of solid ammonia (41) in which the N-D stretching vibration of NH_2D appears as a triplet and the N-H stretching vibration of ND_2H appears as a single broad band. The broad peaks at 3125 and 3050 cm^{-1} in the spectrum of $2ND_3 \cdot D_2O$ (5% H) are assigned to the O-H stretching vibrations of O-H$\cdots$N$_{II}$ and O-H$\cdots$N$_I$, respectively. The isolated O-H stretching vibration which appears as a shoulder at 3050 cm^{-1} corresponds to a strong peak at 2275 cm^{-1} in the isolated O-D stretching region. Although unusual, this same phenomenon occurs in the infrared spectrum of hexamethylenetetramine hexahydrate (1) for the O-H$\cdots$N bond.

The frequencies of the O-H stretching vibrations of HOD do not coincide with the frequencies of the O-H stretching vibrations of H_2O and the frequencies of the O-D stretching vibrations of HOD do not coincide with those of D_2O. These frequencies are close enough, however, to show that coupling between the vibrations of the different

OH (or OD) bonds is small (1) and that the H_2O (or D_2O)
features at 3125 and 2975 cm^{-1} (or 2355 and 2230 cm^{-1}) do
each arise primarily from one O-H···N (or O-D···N) bond of
a particular length and not from a mixture of both. That
is, their assignment under the site group, rather than
under the unit cell group, is valid.

The only other features which arise due to the hydro-
gen impurity are those at 962 and 936 cm^{-1} which are as-
signed to the symmetric deformation of ND_2H, as discussed
above for $2NH_3 \cdot H_2O$ (10% D).

The two sharp peaks at 2445 and 2432 cm^{-1} in the
spectrum of $2NH_3 \cdot H_2O$ (5 or 10% D) are assigned to the iso-
lated stretching vibrations of N_IH_2D which is hydrogen
bonded, while the higher-frequency features at 2501/2490/
2473/2461 cm^{-1} are assigned to $N_{II}H_2D$ which is not hydrogen
bonded. Since N_ID_3 forms two non-equivalent N_I-D···O
bonds, one of length 3.11 Å and two of length 3.24 Å, it
is expected that the vibration of N_IH_2D with its D atom in
the 3.24 Å bond will produce a band to high frequency, and
with twice the intensity of the band due to the vibration
of N_IH_2D with its D atom in the 3.11 Å bond. However, the
two bands appear to have nearly equal intensities, not the
intensity ratio 2:1 (Figure 3.6). This does not necessar-
ily invalidate the assignment since the lower-frequency
band is due to the stronger hydrogen bond and the intrinsic
intensity of an X-H vibration in an X-H···Y bond increases

with hydrogen bond strength, so the prediction of the intensity relation is not straightforward (71,72).

Since the hydrogen atoms in the type II ammonia molecule are unbound, the intensity of the absorption by the $N_{II}H_2D$ vibrations is expected to be weaker than that of N_IH_2D as is observed in Figure 3.6. The appearance of four features may be understood if it is assumed that the hydrogen atoms of $N_{II}H_3$ occupy the two possible orientations which preserve the plane of symmetry. The relative intensities of the four features (5% D curve in Figure 3.6) compare well with the relative intensities expected for this assignment previously discussed in this section. The assignment of the four peaks cannot be made definitively, because there is no evidence to indicate whether 2501 and 2490 cm^{-1} correspond to one orientation while 2473 and 2461 cm^{-1} correspond to the other, or whether the pairing should be 2501/2473 and 2490/2461 cm^{-1}.

A summary of the detailed assignments is given in Table 5.5.

A more detailed assignment (Table 5.5) of the coupled N-D stretching vibration of $2ND_3 \cdot D_2O$ may be made from the above assignment plus the spectra of solid ammonia (41). In the spectra of solid ammonia, the separation of the peaks due to the antisymmetric N-D stretching vibrations of ND_3 and the N-D stretching vibration of NH_2D is approx-

TABLE 5.5

Detailed Assignments of the Absorption by the Stretching

and Symmetric Deformation Vibrations of Ammonia Hemihydrate

Assignments Stretching Vibrations	$2ND_3 \cdot D_2O$ (5%H) $\nu(X-H)/cm^{-1}$	$2NH_3 \cdot H_2O$ (5%D) $\nu(X-D)/cm^{-1}$	$2NH_3 \cdot H_2O$ $\nu(X-H)/cm^{-1}$	$2ND_3 \cdot D_2O$ $\nu(X-D)/cm^{-1}$
$O-H \cdots N_I$ (2.82 Å)	3050	2275	2975	2230
$O-H \cdots N_{II}$ (2.84 Å)	3125	2347	3125	2355
$N_IH \cdots O$ (3.11 Å)	3308	2432	3374	2502
$N_IH \cdots O$ (3.24 Å)	3322	2445		
$N_{II}-H$	3355	2461(1)*	3397	2530
		2473(2)		
		2490(2)		
		2501(1)		
Deformation Vibrations				
$\nu_2(N_IH_2D)$ } C_s or C_1		1056	—	
+ $\nu_2(N_{II}H_2D)$ } C_1 or C_s		1021		
$\nu_2(N_ID_2H)$ } C_s or C_1	962			
+ $\nu_2(N_{II}D_2H)$ } C_1 or C_s	936			
$\nu_2(N_IH_3)$ } $2B_{1u} + 2B_{3u}$			1092	
+ $\nu_2(N_{II}H_3)$ }			1083	
$\nu_2(N_ID_3)$ } $2B_{1u} + 2B_{3u}$				848
+ $\nu_2(N_{II}D_3)$ }				838

*The number in brackets is the relative multiplicity of the site.

imately 60 cm^{-1}. The corresponding splittings in ammonia hemihydrate between the coupled ν_3(N-D) vibrations at 2530 and 2502 cm^{-1} and the average frequency of the isolated N_ID stretching vibrations are 91 and 63 cm^{-1}, respectively. The 2502 cm^{-1} peak may, therefore, be assigned to the antisymmetric N_ID stretch of $N_I D_3$. The splittings observed between the coupled ν_3(N-D) vibrations at 2530 and 2502 cm^{-1} and the average frequency of the four features due to the isolated N_{II}D stretching vibrations are 49 and 21 cm^{-1}, respectively. Therefore, the 2530 cm^{-1} peak is assigned to the antisymmetric N_{II}D stretch of $N_{II}D_3$.

By analogy with the absorption by the isolated N-D vibrations, (Figure 3.6) the two sharp features at 3322 and 3308 cm^{-1} in the spectra of $2ND_3 \cdot D_2O$ (1 or 5% H) (Figure 3.10) are assigned to the isolated N-H stretching vibrations of $N_I D_2 H$ in the 3.24 and 3.11 Å N-H···O bonds (Table 5.5). The splittings observed between the average frequency of this doublet and the coupled ν_3(N-H) vibrations at 3397 and 3374 cm^{-1} in the spectrum of $2NH_3 \cdot H_2O$ are 82 and 59 cm^{-1}, respectively. In solid ammonia, there is a separation of about 44 cm^{-1} between the peaks of the isolated and the coupled antisymmetric N-H stretching vibrations. Therefore, the 3374 cm^{-1} feature is assigned (Table 5.5) to the antisymmetric N_IH stretch of $N_I H_3$. It is assumed that the unresolved peak at 3355 cm^{-1} (Figure

3.10) is due to the isolated N-H stretching vibration of $N_{II}D_2H$. The splittings observed between this peak and those at 3397 and 3374 cm^{-1} are 42 and 19 cm^{-1}, respectively. On this basis, the 3397 cm^{-1} feature is assigned (Table 5.5) to the antisymmetric $N_{II}H$ stretch of $N_{II}H_3$.

It is, thus, concluded that the doublets at 3397/3374 cm^{-1} in the spectrum of $2NH_3 \cdot H_2O$ and 2530/2502 cm^{-1} in the spectrum of $2ND_3 \cdot D_2O$ are due to the multiple-site splitting, that is, to the two different types of ammonia molecules in the structure, and not to site splitting, that is, to the loss of degeneracy of the doubly degenerate ν_3 vibration of the C_{3v} ammonia molecule under the C_s site group. This conclusion is supported by the following calculations which argue strongly against the site splitting interpretation. Using the diatomic molecule approximation (50), force constants were calculated from the isolated N_I-D stretching frequencies 2432 and 2445 cm^{-1} as assigned above (Table 5.5). These force constants were then used to calculate the frequencies of the coupled antisymmetric and symmetric stretching vibrations for NH_3 and ND_3 molecules assuming C_s symmetry. The calculations predict the frequencies of $\nu_3(A')$ and $\nu_3(A'')$ to differ by 11 cm^{-1} for NH_3 and 9 cm^{-1} for ND_3, which is much too small to explain the observed differences of 23 cm^{-1} and 28 cm^{-1}, respectively. The calculations also predicted the coupled symmetric N-H and N-D stretching

vibrations to occur at 3274 and 2350 cm^{-1}, respectively, although these features are not observed in the spectra.

The information obtained from the isolated deformation modes, at 1056/1021 cm^{-1} for NH_2D and 962/936 cm^{-1} for ND_2H, may be used to interpret the observed splittings of the ν_2 modes in the spectra of $2NH_3 \cdot H_2O$ at 1092/1083 cm^{-1} and of $2ND_3 \cdot D_2O$ at 848/838 cm^{-1}. For each ammonia molecule in the neat compounds, there are two infrared active ν_2 modes, $B_{1u} + B_{3u}$, under the unit cell group. Therefore, the observed splitting of $\nu_2(NH_3)$ and $\nu_2(ND_3)$ may be unit-cell-group splitting (due to vibrational coupling) or multiple-site splitting (due to the two types of ammonia molecules). The larger splitting of ~30 cm^{-1} for the isolated deformation vibrations of NH_2D and ND_2H suggests that for these species the splitting is site splitting, that is, due to two different hydrogen sites within a molecule.

The spectra presented in Figure 3.8 show that the 1083 cm^{-1} peak of $2NH_3 \cdot H_2O$ becomes a shoulder in the spectrum of 5% D, and disappears in the spectrum of 10% D, as the 1092 cm^{-1} peak appears to broaden. This effect is indicative of unit-cell-group splitting (34). The deuterium impurity disrupts the selection rules and activates all of the coupled components of ν_2, which broadens the peak. The same broadening is suggested, but less clearly, in the spectra of $2ND_3 \cdot D_2O$ (1 and 5% H).

Several calculations were performed to gain further information about the expected splittings of the symmetric deformation vibration when 1) two quite different but quite symmetric ammonia molecules exist in the structure and 2) two quite similar but quite unsymmetric ammonia molecules exist in the structure. These calculations are summarized in Table 5.6. The interactions between stretching and deformation vibrations were ignored. Separate calculations were made for the four molecules of C_s symmetry, NH_3, NH_2D, ND_2H and ND_3, and for the two molecules of C_1 symmetry, NH_2D and ND_2H, which are shown in projection in the table. The departure of the molecular geometry from the C_{3v} geometry of the gas phase is unknown and was neglected. The force constants were first estimated from the frequencies of ν_2 and ν_4 of NH_3 and ND_3 in the hemihydrate, assuming C_{3v} symmetry for the NH_3 (or ND_3), as shown in the table, and were then adjusted rather arbitrarily to mimic the two cases described above. As shown in Table 5.6, for case 1, the two diagonal force constants (F_{11} and F_{22}) within a molecule differed by 1% while corresponding force constants in the two molecules differed by ~15%. For case 2, the 15% difference was intramolecular and the intermolecular difference was 2%. Thus, calculations were made for 6 molecules with 4 force fields to yield the results shown in Table 5.6.

TABLE 5.6

Summary of Normal Coordinate Calculations of the

Deformation Vibrations of Ammonia

Molecules: The dashed line represents the crystal symmetry plane.
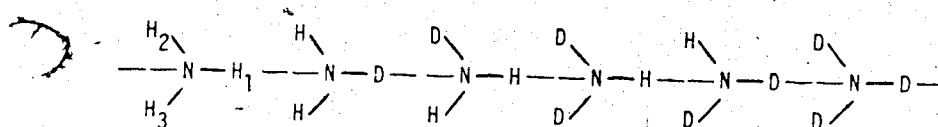
Symmetry: C_s C_s C_1 C_s C_1 C_s

Molecular Geometry: All HNH angles = 106.8°. All N-H distances = 1.01 Å.
The same geometry and atom numbering scheme was used for all isotopic
species.

Displacement Coordinates: $\phi_1 = \Delta \widehat{H_2 N H_3}$, $\phi_2 = \Delta \widehat{H_1 N H_3}$, $\phi_3 = \Delta \widehat{H_1 N H_2}$

Potential Energy: $V = \tfrac{1}{2} [F_{11}\phi_1^2 + F_{22}(\phi_2^2 + \phi_3^2) + 2 F_{23} \phi_2 \phi_3 + 2 F_{12} (\phi_1\phi_2 + \phi_1\phi_3)]$

Force Constants:

For NH_3, symmetry C_{3v}, calculated from $\nu_2 = 1090$ cm^{-1} and
$\nu_4 = 1590$ cm^{-1} via Table 3.4:
$$F_{11} = F_{22} = 0.5669 \text{ mdyne Å}; \quad F_{12} = F_{23} = -0.0278 \text{ mdyne Å}$$

For ND_3, symmetry C_{3v}, calculated from $\nu_2 = 843$ cm^{-1} and
$\nu_4 = 1170$ cm^{-1} via Table 3.7:

$$F_{11} = F_{22} = 0.5789 \text{ mdyne Å}; \quad F_{12} = F_{23} = -0.0252 \text{ mdyne Å}$$

Table 5.6, continued

Force Constants:

For C_s and C_1 molecules:

Case 1	F_{11} mdyne Å	F_{22} mdyne Å	$F_{23} = F_{12}$ mdyne Å
Molecule 1	0.5192	0.5244	-0.0252
Molecule 2	0.6033	0.6094	-0.0252

Case 2			
Molecule 1	0.5244	0.6094	-0.0252
Molecule 2	0.5140	0.5972	-0.0252

Calculated Frequencies (in cm^{-1}): " indicates the A" mode under C_s.

Case 1	Molecule 1			Molecule 2		
NH_3	1528"	1524	1047	1138	1637	1642"
$NH_2D(C_s)$	1497	1303"	966	1049	1400"	1609
$NH_2D(C_1)$	1501	1300	965	1048	1397	1614
$ND_2H(C_s)$	1372"	1163	873	948	1251	1474"
$ND_2H(C_1)$	1369	1164	875	950	1252	1471
ND_3	1116"	1112	797	865	1195	1199"

Case 2						
NH_3	1642"	1571	1105	1092	1556	1627"
$NH_2D(C_s)$	1533	1400"	1026	1014	1387"	1519
$NH_2D(C_1)$	1604	1354	1014	1003	1341	1588
$ND_2H(C_s)$	1474"	1219	906	896	1208	1460"
$ND_2H(C_1)$	1431	1225	930	919	1213	1417
ND_3	1199"	1148	840	831	1137	1188"

Only the frequencies in the middle two columns of the table appear in the symmetric deformation region. Thus, in case 1 (very different molecules, to mimic multiple-site splitting), NH_3 in the hydrate has the site frequencies 1047/1138 cm^{-1}, split by 91 cm^{-1}, ND_3 has 797/865 cm^{-1}, split by 68 cm^{-1}, while isolated NH_2D should yield four bands at 965/966 and 1048/1049 cm^{-1}, that is, a doublet split by 83 cm^{-1}, and isolated ND_2H should yield 873/875 and 948/950 cm^{-1}, that is, a doublet split by 75 cm^{-1}, where each line of the doublet is itself an un-resolved doublet for NH_2D and ND_2H. Thus, if multiple-site splitting predominates, the splitting of ν_2 in NH_3 and ND_3 should approximately equal that in isolated NH_2D and ND_2H. This is not observed. In case 2 (which mimics similar molecules, each very unsymmetrical), NH_3 and ND_3 have the site frequencies 1105/1092 and 840/831 cm^{-1}, respectively, while isolated NH_2D yields 1026/1014/1014/1003 cm^{-1} and isolated ND_2H yields 906/930/896/919 cm^{-1} which could, at best, appear in the spectra as a triplet for NH_2D and a doublet, at ~900 and 925 cm^{-1} for ND_2H. In this case, the splitting for NH_3 and ND_3 is much less than for NH_2D and ND_2H, as is observed, but the observation of a doublet for NH_2D as well as a doublet for ND_2H can only occur by accident. Thus, these calculations indicate that case 1 can only explain the observations if the vib-rations of one of the two molecules absorb quite strongly

as NH_2D and ND_2H but have not been detected for NH_3 and ND_3. This is believed to be unlikely. The calculations indicate that case 2 can explain the fact that only doublets were observed for NH_2D and ND_2H if the two types of molecules have virtually identical HNH (or HND or DND) deformation frequencies. This is believed to be the explanation of the absorption by NH_2D and ND_2H, while the doublet seen for NH_3 and ND_3 is believed to arise from unit-cell-group splitting (intermolecular vibrational coupling), as described earlier. Further, the calculations support the tentative conclusion drawn earlier that the peaks at 1156 cm^{-1} in $2NH_3 \cdot H_2O$ and at 884 cm^{-1} in $2ND_3 \cdot D_2O$ are not due to the symmetric deformation of ammonia.

It should be noted that this interpretation implies that the type I and II molecules are practically identical with respect to their deformation vibrations while it was concluded earlier that they are quite dissimilar with respect to their stretching vibrations. On the grounds that hydrogen bonding affects stretching vibrations more than deformation vibrations, this is quite possible.

The assignments that are believed to be correct are summarized in Table 5.5.

CHAPTER VI.

CONCLUSION

In the course of this work, the mid-infrared spectra of authentic samples of ammonia monohydrate and ammonia hemihydrate have been characterized, thus revising the literature (5) of 27 years ago. The assignment of 3012 cm^{-1} to the 2.81 Å O-H$\cdots$N bond of hexamethylenetetramine hexahydrate (1) has been confirmed by the spectra of the ammonia hydrates. These spectra show that the absorption by O-H stretching vibrations of O-H$\cdots$N bonds of length 2.775 to 2.85 Å at 95°K appear between 2910 and 3125 cm^{-1}.

The assignment of the spectral features of the ammonia hydrates has been made as far as the spectral evidence allows. As a result of this study, several interesting questions have arisen concerning the origin of the splittings observed in the spectra of ammonia hemihydrate. Although plausible assignments have been made on the basis of the data obtained, further evidence is required to definitively interpret the spectra. For example, a study of the temperature dependence of the infrared spectrum may indicate clearly which spectral features are due to N_IH_3 and to $N_{II}H_3$ in the hemihydrate because if the sample is cooled below the 52°K transition, the $N_{II}H_3$ would freeze in an ordered arrangement or if the sample was heated, the disorder of the $N_{II}H_3$ may increase, causing

spectral changes. The Raman spectra of the hydrates should add evidence about the influence of intermolecular coupling, particularly for the centrosymmetric hemihydrate. Finally, the far-infrared and low-frequency Raman spectra should provide clear evidence about the disorder in the structures.
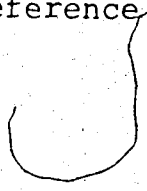
REFERENCES

1. J.E. Bertie and M. Solinas. Can. J. Chem. 53, 2624 (1975).

2. K. Nakamoto, M. Margoshes and R.E. Rundle. J. Amer. Chem. Soc. 77, 6480 (1955).

3. I. Olovsson and D.H. Templeton. Acta Cryst. 12, 827 (1959).

4. W.J. Siemons and D.H. Templeton. Acta Cryst. 7, 194 (1954).

5. R.D. Waldron and D.F. Hornig. J. Amer. Chem. Soc. 75, 6079 (1953).

6. D.L. Hildenbrand and W.F. Giauque. J. Amer. Chem. Soc. 75, 2811 (1953).

7. F.F. Rupert. J. Amer. Chem. Soc. 31, 866 (1909).

8. F.F. Rupert. J. Amer. Chem. Soc. 32, 748 (1910).

9. A. Smits and S. Postma. Wisk en Natk. Afd. 18, 94, thru Chem. Zentr., I, 1217 (1910).

10. A. Smits and S. Postma. Verslag Akad. Wetenschappen 23, 110 (1914).

11. G. Baume and A. Tykociner. J. Chim. Phys. 12, 270 (1914).

12. S. Postma. Rec. trav. chim. Pays-Bas 39, 515 (1920).

13. L.D. Elliott. J. Phys. Chem. 28, 887 (1924).

14. K.E. Mironov. Zhur Obshchei. Khim. 25, 1081 (1955).

15. A.P. Rollet and G. Vuillard. C.R. Acad. Sci. 243, 383 (1956).

16. G. Vuillard. Ann. de Chim. Series 13 $\underline{2}$, 233 (1957).

17. F. Friedrichs. Z. anorg. allgem. Chem. $\underline{127}$, 228 (1923).

18. P.H.G. Van Kasteren. Bull. Inst. Int. Froid, Annexe $\underline{4}$, 81 (1973).

19. International Tables for X-Ray Crystallography, 2nd Edition. Vol. 1. Edited by F. Henry and K. Lonsdale. T. Kynoch Press, Birmingham, 1965.

20. F.A. Cotton and G. Wilkinson. Advanced Inorganic Chemistry, 3rd edition. Interscience Publishers, New York, 1972, p. 160.

21. S. Eletr and C.T. O'Konski. J. Chem. Phys. $\underline{54}$, 4312 (1971).

22. J.E. Bertie and E. Whalley. Spectrochim. Acta $\underline{20}$, 1349 (1964).

23. Handbook of Chemistry and Physics, 56th edition. Edited by R.C. Weast. CRC Press, Inc., 1975.

24. T.C. Waddington. Non-Aqueous Solvent Systems. Academic Press, New York, 1965, p. 4.

25. E.W. Nuffield. X-ray Diffraction Methods. J. Wiley and Sons Inc., New York, 1966, p. 34.

26. F.E. Bates. Ph.D. thesis, University of Alberta, 1978.

27. B. Post, R.S. Schwartz and I. Fankuchen. Rev. Sci. Instr. $\underline{22}$, 218 (1951).

28. T.B. Reed and W.N. Lipscomb. Acta Cryst. $\underline{6}$, 45 (1953).

29. K. Simpson. Ph.D. thesis, University of Alberta, 1973.

30. I.U.P.A.C. Tables of Wavenumbers for the Calibration of Infrared Spectrometers, 2nd edition. Compiled by A.R.H. Cole. Pergamon Press, New York, 1977.

31. J.E. Bertie, L.D. Calvert and E. Whalley. Can. J. Chem. 42, 1373 (1964).

32. I. Olovsson and D.H. Templeton. Acta Cryst. 12, 832 (1959).

33. Reference 25, pp. 107-111.

34. J.E. Bertie. 'Infrared Spectra of Solids at Normal and High Pressures' in Proc. NATO Adv. Study Inst., Florence, Italy, 1980. Edited by J.R. Durig, D. Reidel, Dordrecht, 1980.

35. G. Turrell. Infrared and Raman Spectra of Crystals. Academic Press, London, 1972, p. 48.

36. J.C. Decius and R.M. Hexter. Molecular Vibrations in Crystals. McGraw-Hill, New York, 1977, p. 44.

37. W.G. Fateley, F.R. Dollish, N.T. McDevitt and F.F. Bentley. Infrared and Raman Selection Rules for Molecular and Lattice Vibrations: The Correlation Method. Wiley-Interscience, New York, 1972.

38. G. Herzberg. Molecular Spectra and Molecular Structure II. Infrared and Raman Spectra of Polyatomic Molecules. Van Nostrand Reinhold Company, New York, 1945, pp. 280-282 and 294-297.

39. F.P. Reding and D.F. Hornig. J. Chem. Phys. 19, 594 (1951).

40. F.P. Reding and D.F. Hornig. J. Chem. Phys. 23, 1053 (1955).

41. H. Wolff, H.-G. Rollar and E. Wolff. J. Chem. Phys. 55, 1373 (1971).

42. O.S. Binbrek and A. Anderson. Chem. Phys. Letters 15, 421 (1972).

43. A. Bromberg, S. Kimel and A. Ron. Chem. Phys. Letters 46, 262 (1977).

44. J.E. Bertie and E. Whalley. J. Chem. Phys. 40, 1637 (1964).

45. M.S. Bergren, D. Schuh, M.G. Sceats and S.A. Rice. J. Chem. Phys. 69, 3477 (1978).

46. J.W. Reed and P.M. Harris. J. Chem. Phys. 35, 1730 (1961).

47. A.W. Hewat and C. Riekel. Acta Cryst. A 35, 569 (1979).

48. M. Falk and O. Knop. In Water. A Comprehensive Treatise. Vol. 2. Edited by F. Franks. Plenum Press, New York, 1973, Chapt. 2, p. 105.

49. L. Pauling. The Nature of the Chemical Bond, 3rd edition. Cornell University Press, New York, 1960, p. 260.

50. L.A. Woodward. Introduction to the Theory of Molecular Vibrations and Vibrational Spectroscopy. Oxford University Press, London, 1972.

51. E.B. Wilson Jr., J.C. Decius and P.C. Cross. Molecular Vibrations. McGraw-Hill Book Company, New York, 1955, p. 332.

52. D. Hadzi and S. Bratos. In The Hydrogen Bond, Recent Developments in Theory and Experiments. Vol. 2. Edited by P. Schuster, G. Zundel and C. Sandorfy. North Holland, Amsterdam, 1976, p. 574.

53. J.R. Scherer. In Advances in Infrared and Raman Spectroscopy. Vol. 5. Edited by R.J.H. Clarke and R.E. Hester. Heyden, London, 1978, p. 149.

54. B. Berglund, J. Lindgren and J. Tegenfeldt. J. Mol. Struct. 43, 179 (1978).

55. Reference 51, p. 184.

56. R. McGraw, W.G. Madden, M.S. Bergren, S.A. Rice and M.G. Sceats. J. Chem. Phys. 69, 3483 (1978).

57. J.E. Bertie and F.E. Bates. J. Chem. Phys. 67, 1511 (1977).

58. J.E. Bertie and B.F. Francis. J. Chem. Phys. 72, 2213 (1980).

59. J.E. Bertie and E. Whalley. J. Chem. Phys. 40, 1646 (1964).

60. J.E. Bertie. Appl. Spectrosc. 22, 634 (1968).

61. J.E. Bertie, F.E. Bates and D.K. Hendrickson. Can. J. Chem. 53, 71 (1975).

62. H.J. Hrostowski and G.C. Pimentel. J. Chem. Phys. 19, 661 (1951).

63. G.L. Hiebert and D.F. Hornig. J. Chem. Phys. 20, 918 (1952).

64. Reference 38, p. 265.

65. Reference 51, p. 74.

66. Reference 51, p. 303.

67. J.R. Scherer and R.G. Snyder. J. Chem. Phys. 67, 4794 (1977).

68. J.E. Bertie, H.J. Labbe and E. Whalley. J. Chem. Phys. 50, 4501 (1969).

69. J.C. Evans. Spectrochim. Acta. 16, 994 (1960).

70. J.C. Evans. Spectrochim. Acta. 18, 507 (1962).

71. G.C. Pimentel and A.L. McClellan. The Hydrogen Bond. W.H. Freeman and Company, San Francisco, 1960, p. 95.

72. Reference 52, p. 576.

APPENDIX

Parameters of Nicolet 7199 FTIR Spectrometer

Used to Obtain Spectra Presented in this Thesis

Parameter	Value	Meaning
FSZ	22528	File size of data blocks on scratch pad disk.
NDP	16384	Number of data points collected per scan. At SSP = 2, this corresponds to 1 cm^{-1} resolution.
NTP	32768	Number of points Fourier transformed, i.e. 16384 zero points were added to the data points before Fourier transformation.
NSS	500	Number of sample scans, i.e. number of interferograms averaged before Fourier transformation.
NSB	500	Number of background scans, as for NSS.
GAN	4	Gain of amplifier board.
SGL	1	Gain given by GAN for the first 1024 data points and by SGH times GAN for the remainder.
SGH	8	
AFN	HG	Happ-Genzel Apodization used for all spectra.
HPS	0	High- and Low- pass electronic filters set with 3 dB points at 10 Hz and 50 kHz.
LPS	6	
VEL	36	Mirror velocity equals 0.90 cm sec^{-1}.
NSK	0	Number of points skipped between white light signal and the start of data collection. The zero path position is the (451 - NSK) data point.
COR	LO	Each interferogram was correlated with those previously collected and adjusted one data point in either direction to make the peaks match, before signal averaging.

Parameter	Value	Meaning
SSP	2	Path-difference increment between data points equals (0.3164957 μm x n x SSP) where 0.3164957 is half the wavelength of the He-Ne laser and n is the refractive index of air at 632.9 nm.
APT	FL	Source aperture diameter, FL = 6.3 mm MD = 2.3 mm SM = 1.1 mm; Intensity ratios are 100:32:8
NPD	200	Number of data points used in phase calculation; 100 data points on each side of the zero-path-position were used.
NPT	1024	Number of transform points used in phase calculation; NPT-NPD = 824 zero points were added before Fourier transformation.
PHZ	PH	The real part of the phase-corrected transform was calculated as the spectrum.